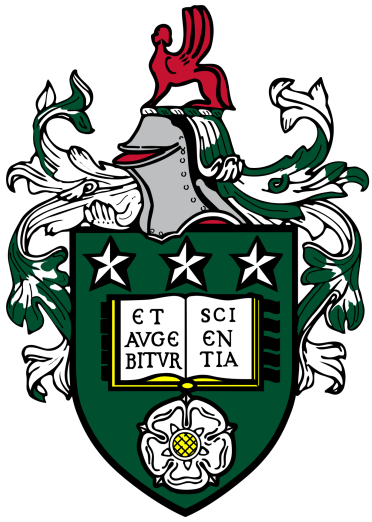

Edge States in a Relativistic Description of Carbon Nanotubes

Benjamin Christopher Duggan

Submitted in accordance with the requirements for the degree of
Master of Science by Research

The University of Leeds

School of Physics and Astronomy

September 2021

Intellectual Property

The candidate confirms that the work submitted is his own and that appropriate credit has been given where reference has been made to the work of others.

Acknowledgements

I am extremely grateful for the guidance and advice of my supervisor, Prof Jiannis K. Pachos, and that of his PhD student, Matthew Horner. They have offered me an immeasurable amount of insight and knowledge, without which I could not have hoped to understand my research topic so well.

I would also like to thank my friends who I have lived with for the past year, and my family for their continuous support during this degree, which has coincided with two national lockdowns during the COVID-19 pandemic. They have kept me happy, sane and focussed during these difficult times.

Abstract

Graphene based systems admit a relativistic description in their low energy sector. This is due to the linear dispersion around the systems Dirac points. At such low energies where the dispersion is linear, support for bulk states at the edges of zigzag carbon nanotubes has been theoretically demonstrated. This is due to the wavefunctions of the two triangular sub-lattices being out of phase for certain system configurations, and the less stringent boundary conditions applied to relativistic systems. We demonstrate that no such theoretical support for bulk states at the edge is found for armchair carbon nanotubes. Instead, it is shown that the armchair carbon nanotube exhibits non-relativistic results where the charge density necessarily goes to zero at the edge, as would be expected in a system that admitted a Schrödinger description. These results are explained in terms of the shape of the edges and the resultant boundary conditions that we use when solving the Dirac equation for both zigzag and armchair systems in their low energy limit. The shape of the armchair edge requires that the wavefunctions of both sub-lattices equal zero at the edge and therefore, the density must be zero at the edge as well.

Contents

1 Introduction **1**

2 The Honeycomb Lattice of Graphene **3**

3 The Klein Paradox **4**
3.1 Relativistic Particle Incident on a Potential Barrier 5
3.2 The Klein Paradox in Single-Layer Graphene 9

4 The Tight-Binding Model **10**
4.1 Second Quantisation 11
4.2 The Tight-Binding Hamiltonian for Graphene 14

5 The Dispersion Relation for Graphene **17**

6 Review of Edge States in Zigzag Carbon Nanotubes **19**
6.1 Zigzag Momentum Quantisation and Dispersion Relation 19
6.2 Support of Bulk States at the Edge 21

7 Analysis of Armchair Carbon Nanotubes **23**
7.1 Armchair Momentum Quantisation and Dispersion Relation 24
7.2 Wavefunctions for the Armchair Carbon Nanotube 25
7.3 Charge Density at the Edge 27

8 Numerical Simulation of a 1D Chain **28**

9 Conclusion **31**

References **31**

A Source Code for Plots and Numerics **34**
A.1 Graphene Dispersion Relation Plot 34
A.2 Armchair Carbon Nanotube Dispersion Relation Plot 35
A.3 Ground State Energy Band with Minima Plot 36
A.4 Numerical Simulation of a 1D Chain 37

List of Figures

1 The Hexagonal Lattice of Graphene with Armchair and Zigzag Boundaries . . . 1
2 Graphene Lattice with Unit Vectors and Sub-Lattices Defined 3
3 Relativistic Particle Incident on a Potential Barrier 5
4 Graphene Lattice with Unit Cell Hopping 16
5 2D Dispersion Relation for Graphene 18
6 Numerical Simulation of a Zigzag Carbon Nanotube 23
7 Dispersion Relation for an Armchair Carbon Nanotube 25
8 Energy Band for the Ground State of an Armchair Carbon Nanotube 26
9 Graphene with Unit Cell Hopping in a Cartesian Basis 29
10 Numerical Simulation of an Armchair Carbon Nanotube 30

1 Introduction

Carbon nanotubes are made from a single-atomic layer of carbon, known as graphene, wrapped around into a tube. Graphene has a hexagonal lattice structure with carbon atoms at its vertices and has the unusual property that its quasiparticle excitations behave according to the Dirac equation in a way similar to electrons [1]. As the Dirac Equation is relativistic, its use in the description of graphene predicts the emergence of certain relativistic phenomena, such as the Klein paradox [1] and the existence of edge states on the boundary of zigzag carbon nanotubes [2].

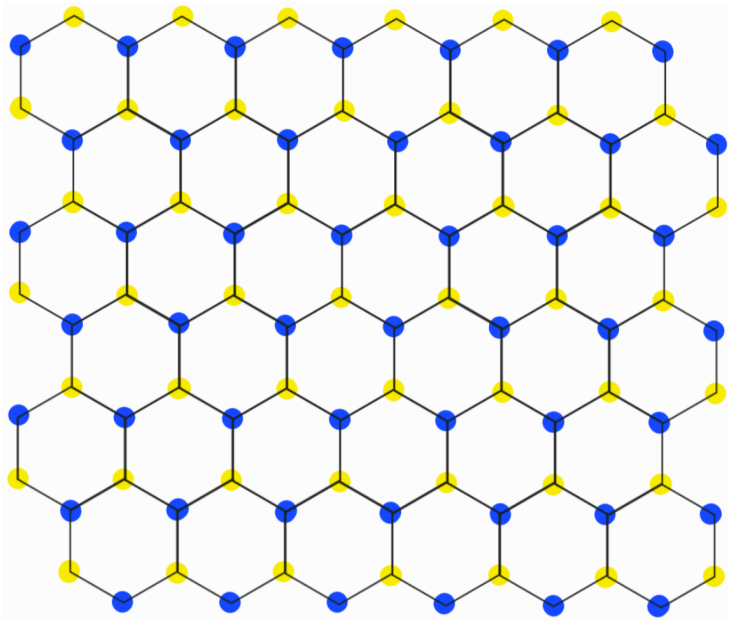

Figure 1: The hexagonal lattice of graphene with armchair boundaries visible on the vertical edges and zigzag boundaries along the horizontal edges. This hexagonal lattice can be divided into two triangular sub-lattices, coloured yellow and blue respectively.

The aim of this thesis is to analyse the emergence of similar relativistic effects in carbon nanotubes with armchair boundaries rather than zigzag. This difference in boundary shape is due to the angle one chooses to cut the graphene boundary at. If we have an armchair boundary, then a zigzag boundary is a 30° rotation from that in either direction. We then find another armchair boundary a 30° rotation after that, and this sequence repeats all around in a circle. This means that an armchair boundary appears at every 90° angle to a zigzag boundary and vice versa. When we take a quadrilateral sheet of graphene as in fig. 1, and roll it up into a carbon nanotube, we can expect one pair of the parallel sides of the quadrilateral to be armchair and the other zigzag. Then, the boundary of our nanotube simply depends on which two parallel sides we choose to connect. For example, if we connect the zigzag sides to each other, we will have a nanotube with armchair boundaries at is ends.

This thesis will show that carbon nanotubes with the armchair boundary do not support the same relativistic phenomena as the zigzag nanotube. It will also seek to explain why such a small change in the setup of the nanotube can lead to such a large change in the physical properties of the system. The second section of this thesis will introduce the basic geometry of the honeycomb shape of the graphene lattice. The next section will serve to demonstrate how relativistic effects in graphene can lead to counter-intuitive results. The Klein paradox will be used as an example to demonstrate this. The Klein paradox is an usual result of relativistic physics, where a particle incident on an infinite potential barrier, will penetrate with certainty. Unlike the classical case where we would expect any boundary with a potential greater than the energy of the incident particle, to reflect it. The general Klein paradox will be explored before seeing directly how it manifests in graphene.

In section 4, we will build up some fo the background physics needed to study edge states in carbon nanotubes. We will explore methods from many-body quantum mechanics such as the occupation number representation and second quantisation. We will also explore the tight-binding model, which is the appropriate model from condensed matter physics for a system like graphene. Through, this section, our goal will be to derive an appropriate Hamiltonian which can then be used to in our analysis of carbon nanotubes. This will lead onto section 5 where we use this Hamiltonian to derive a general dispersion relation for graphene.

Once we have the dispersion relation for graphene, we can then apply periodic boundary conditions to build carbon nanotubes. In section 6, we will review recent research that suggests there is support for the existence of bulk states at the edge of zigzag carbon nanotubes [2]. This review will consist of looking into how to quantise the momenta in a zigzag carbon nanotube and how this can be used to reduce the general graphene dispersion relation into one for a zigzag carbon nanotube. We will then seek to reproduce the results of [2], so that they can then be directly compared to the analysis of armchair carbon nanotubes later on.

Section 7 will focus on performing a theoretical analysis to see if similar bulk states are supported at the edge of armchair carbon nanotubes. In a similar fashion to the zigzag case, we will quantise the moments in order to derive an armchair dispersion relation. This will allow us to derive the Dirac Hamiltonian for such a system and its eigenstate solutions will be found. After constructing standing wave solutions out of these wavefunctions, the appropriate boundary conditions are applied, in order to to calculate the charge density at the edge. This will demonstrate that there is no such support for bulk states at the edge of an armchair carbon nanotube.

Finally, section 8 will display the results of numerical simulations which support the validity of our theoretical analysis of armchair carbon nanotubes. The numerical simulation of a one dimensional chain using our graphene Hamiltonian will demonstrate that an armchair carbon nanotube is best described by a non-relativistic wavefunction. The results of this thesis will then

be discussed in section 9, where the zigzag and armchair cases will be compared in order to better understand why the two systems, which only appear to be slightly different, manifest different physical results. The different boundary conditions that we use for the armchair and zigzag nanotubes will be used to explain the difference in the support of edge states. The justification for using different sets of boundary conditions will also be explained in order to make sense of these results.

2 The Honeycomb Lattice of Graphene

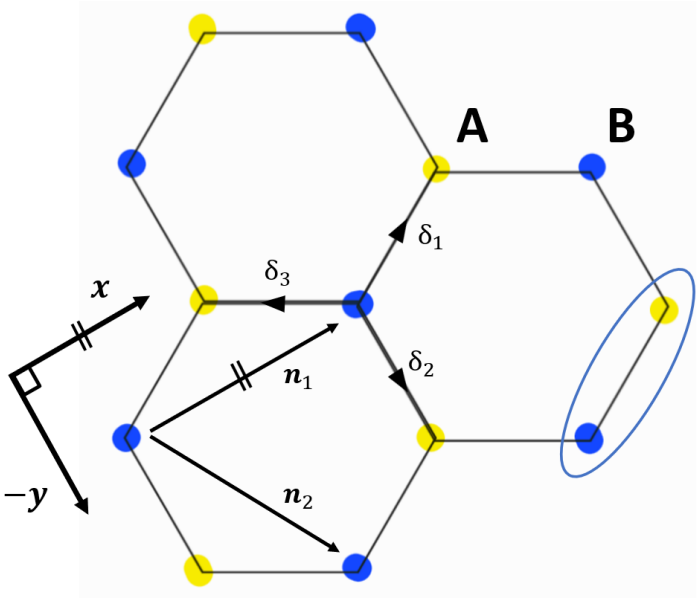

Figure 2: The graphene lattice with the two triangular sub-lattices, A and B shown. We define vectors $\boldsymbol{\delta_1}$, $\boldsymbol{\delta_2}$ and $\boldsymbol{\delta_3}$ between nearest neighbour sites in the hexagonal lattice. A single unit cell of the lattice is enclosed in a blue oval. $\boldsymbol{n_1}$ and $\boldsymbol{n_2}$ are the basis vectors between unit cells, which generates the Bravais lattice of our system. We define $\boldsymbol{n_1}$ to be parallel to the x-direction of our plane. This figure corresponds to eq. (1), eq. (2) and eq. (3).

In order to model graphene, and subsequently a carbon nanotube, we must first describe how to set up the mathematical framework we will use for such a condensed matter system. We will define our coordinate system for the lattice we are describing. Again, we follow the lead of [1] in how we set up our honeycomb lattice. In fig. 2, we divide our lattice into two triangular sub-lattices, A and B. We then choose our unit cell to include one lattice site from each triangular sub-lattice as shown. For simplicity, we have chosen $\boldsymbol{n_1}$ to be parallel to the x-axis. The pair of basis vectors $\boldsymbol{n_1}$ and $\boldsymbol{n_2}$, span the space of lattice sites. This allows us to move between any two unit cells with a vector written in terms of the basis vectors $\boldsymbol{n_i}$. If a is taken to be the lattice

constant given by $a = |\boldsymbol{n_i}|$, then we can see from fig. 2 that we have,

$$\boldsymbol{n_1} = a(1, 0), \quad \boldsymbol{n_2} = \frac{a}{2}(1, -\sqrt{3}). \tag{1}$$

Also, if $b = |\boldsymbol{\delta_i}|$ is the length of the nearest neighbour links, then we get,

$$\boldsymbol{\delta_1} = \frac{b}{2}(\sqrt{3}, 1), \quad \boldsymbol{\delta_2} = b(0, -1), \quad \boldsymbol{\delta_3} = \frac{b}{2}(-\sqrt{3}, 1), \tag{2}$$

as our nearest neighbour vectors. Our choice to make the x-axis parallel to $\boldsymbol{n_1}$ allows us to deduce from inspection that $a = \sqrt{3}b$ because,

$$a = |\boldsymbol{n_i}| = \delta_{1,x} + \delta_{3,x} = (\sqrt{3} \times b) + (0 \times b) = b\sqrt{3}. \tag{3}$$

We can also define the reciprocal lattice to our real space lattice by using the relation $\boldsymbol{G}_i \cdot \boldsymbol{n}_j = 2\pi\delta_{ij}$ [2]. The reciprocal basis vectors, $\boldsymbol{G}_i$ that satisfy this relation are

$$\boldsymbol{G}_1 = \frac{2\pi}{a\sqrt{3}}(\sqrt{3}, 1), \quad \boldsymbol{G}_2 = \frac{2\pi}{a\sqrt{3}}(0, -2). \tag{4}$$

This leads to a two-dimensional, hexagonal reciprocal lattice with Dirac points at its vertices [1]. When the two-dimensional Brillouin zone is plotted against the energy to give the 3D dispersion relation, we see that the allowed energy values crosses through the Dirac points at $E = 0$. More importantly, in the low energy limit around the Dirac points, the dispersion relation appears linear $E \sim k$ instead of the more common quadratic dispersion given by $E \sim k^2$. Famously, non-relativistic phenomena obeys the energy-momentum relation, $E = \boldsymbol{p}^2/2m$, but when considering relativistic physics, we must use $E = \sqrt{(pc)^2 + (m_0c^2)^2}$. We can see that the relativistic energy-momentum relation implies that the energy is proportional to the momentum. Therefore, we can use relativistic physics to describe the low energy properties of graphene systems where $E \sim k$ [1].

3 The Klein Paradox

Before considering the existence of edge states in carbon nanotubes, we will first look at an example of relativistic effects manifesting in graphene. A textbook example of relativistic phenomena in graphene is the Klein paradox, which we will use as an example of the strange consequences that including relativity in our analysis can lead to. The Klein paradox is not really a paradox, but it is a very counter-intuitive result, at odds with both non-relativistic quantum and classical mechanics. The Klein paradox will be explored in two sections with the first, looking at the paradox in a general one-dimensional system. This will serve to demonstrate the effects counter-intuitiveness. We will then look at how it manifests itself in two-dimensional graphene systems, in order to relate it back to the topic of this thesis.

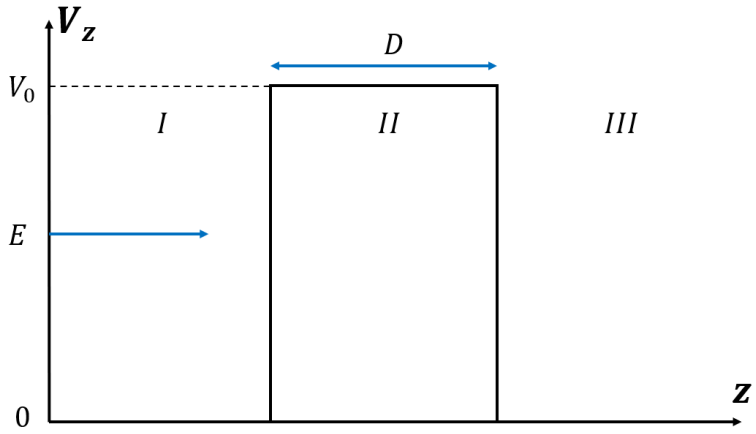

Figure 3: A Dirac fermion of energy, E is moving in the z-direction in region I and is incident on a potential barrier of energy, V_0 represented by region II.

3.1 Relativistic Particle Incident on a Potential Barrier

The Klein paradox occurs when a Dirac fermion approaches a potential barrier. In classical mechanics, the standard result for a particle with $E < V_0$, incident on a potential barrier, V_0 as shown in fig. 3, is that the particle will certainly be reflected by the barrier. On the other hand, non-relativistic quantum mechanics says that there is a probability of the particle "tunnelling" through the barrier, but the probability will decrease as the potential barrier is increased in size [3]. The fact that the particle can tunnel through the barrier at all, is the surprising result from non-relativistic quantum mechanics. However, it is fairly intuitive that the chance of tunnelling will decrease when the barrier gets bigger. This is where the Klein paradox is even more surprising, as when a fermion described by the relativistic Dirac equation approaches a potential barrier, we actually find that the probability of tunnelling increases with the size of the barrier. In fact, one finds that Dirac fermions should pass through the barrier with certainty for an infinite potential [4]. We will now demonstrate how we get these results in a general, one-dimensional system.

In non-relativistic quantum mechanics, the tunnelling phenomenon is demonstrated by considering incident and reflected waves in region I of fig. 3, and a transmitted wave in region II. The wavefunctions in each region can be described as the sum of plane waves. Boundary conditions equating the wave functions at the region boundaries are then applied, which allows one to calculate the reflection and transmission coefficients at each boundary. The transmission coefficient corresponds to the probability of a quantum particle tunnelling through the barrier [5]. We will follow a similar analysis, based off the approach given in [6].

As we are considering a relativistic particle, we will use the Dirac, rather than the Schrödinger equation. The Dirac equation can be written in the form

$$\hat{H}\psi = (\alpha_z p_z c + \beta mc^2)\psi = E\psi, \tag{5}$$

where $p_z = -i\hbar\partial_z$ is the z-component of the momentum operator, and we have

$$\alpha_z = \begin{pmatrix} 0 & \sigma_z \\ \sigma_z & 0 \end{pmatrix} = \begin{pmatrix} 0 & 0 & 1 & 0 \\ 0 & 0 & 0 & -1 \\ 1 & 0 & 0 & 0 \\ 0 & -1 & 0 & 0 \end{pmatrix}, \quad \beta = \begin{pmatrix} I_2 & 0 \\ 0 & -I_2 \end{pmatrix} = \begin{pmatrix} 1 & 0 & 0 & 0 \\ 0 & 1 & 0 & 0 \\ 1 & 0 & -1 & 0 \\ 0 & 0 & 0 & -1 \end{pmatrix}, \tag{6}$$

where we have introduced block matrix notation. From eq. (5), we can deduce the following equation and it's adjoint as

$$(E - \beta mc^2 - \alpha pc)\psi = \left(\frac{E}{c} - \beta mc\right)\psi + i\hbar\alpha\frac{\partial\psi}{\partial z} = 0 \tag{7}$$

and

$$\bar{\psi}(E - \beta mc^2 - \alpha pc) = \bar{\psi}\left(\frac{E}{c} - \beta mc\right) + i\hbar\frac{\partial\bar{\psi}}{\partial z}\alpha = 0 \tag{8}$$

where we have dropped the z index for α and p, as we are restricting ourselves to one dimension, so it is implicit. For a free Dirac fermion, we have

$$\left(\frac{E}{c}\right)^2 = p^2 + m_0^2c^2, \tag{9}$$

which becomes,

$$\left(\frac{E-V}{c}\right)^2 = \bar{p}^2 + m_0^2c^2, \tag{10}$$

in the presence of a constant potential, V [6]. In the region of constant potential, we can expect the momentum to be different to the free particle case. Therefore, we introduce $\bar{p}$ as the momentum inside the barrier. We can substitute this back into eq. (7) (and eq. (8)) to get the Dirac equation for a particle in a constant potential,

$$\left(\frac{E-V}{c} - \beta m_0 c\right)\psi + i\hbar\alpha\frac{\partial\psi}{\partial z} = 0. \tag{11}$$

The adjoint for this equation can be found analogously as

$$\bar{\psi}\left(\frac{E-V}{c} - \beta m_0 c\right) + i\hbar\frac{\partial\bar{\psi}}{\partial z}\alpha = 0. \tag{12}$$

Now that we have a Dirac equation for a free particle and for one in a constant potential, we can describe our system as shown in fig. 3. Using the fact that the potential $V = V(z)$ is given

by

$$V(z) = \begin{cases} 0 & \text{in region } I, \\ V_0 & \text{in region } II, \\ 0 & \text{in region } III, \end{cases} \tag{13}$$

we can now begin to analyse what the wavefunctions in each region will look like. We can assume that the wavefunctions take the form of plane waves. Therefore, we can assume that our incident wave on the barrier will take the form

$$\psi_i = u_i \exp\left\{\frac{i}{\hbar}(pz - Et)\right\}, \tag{14}$$

as given in [6]. We can now substitute this back into the Dirac equation (eq. (7)) and simplify to get

$$\left(\frac{E}{c} - \beta m_0 c - \alpha p\right) u_i = 0, \tag{15}$$

which describes a wave, u_i incident on the barrier with momentum, $+p$. By conservation of momentum, we can assume that a reflected particle would have momentum, $-p$. We also know that the momentum of the transmitted wave will be $\bar{p}$. This allows us to define plane waves for the reflected and transmitted components and analogously deduce that,

$$\left(\frac{E}{c} - \beta m_0 c + \alpha p\right) u_r = 0, \tag{16}$$

and

$$\left(\frac{E - V_0}{c} - \beta m_0 c - \alpha \bar{p}\right) u_t = 0. \tag{17}$$

We are now in a position to apply our boundary conditions. At the beginning of this section, we discussed how in non-relativistic quantum mechanics, one requires the overall wavefunction to be continuous at the boundary. However, in the relativistic case, we only need to equate the wavefunctions at the boundary [1]. This is a less stringent condition than requiring continuity, where the derivatives of the wavefunction must also be equal at the boundary. By doing this to our system between regions I and II, we require that

$$u_i + u_r = u_t, \tag{18}$$

where the L.H.S. represents the incident and reflected waves in region I, and the R.H.S. represents the transmitted wave moving through the barrier in region II. Our aim is to use these boundary conditions to calculate the probability current at the boundaries, as this will give us the probability of reflection or transmission through the barrier.

In region I, if we take the sum of eq. (15) and eq. (16), and then rearrange our expression, we get

$$\left(\frac{E}{c} - \beta m_0 c\right)(u_i + u_r) = \alpha p(u_i - u_r). \tag{19}$$

Similarly, if we take eq. (17), we can rearrange it using eq. (18) to substitute $(u_i + u_r)$ for u_t and then rearrange to get

$$\left(\frac{E}{c} - \beta m_0 c\right)(u_i + u_r) = \left(\frac{V_0}{c} + \alpha\bar{p}\right)(u_i + u_r). \tag{20}$$

We can now equate the L.H.S. of eq. (19) and eq. (20), so that we have

$$\left(\frac{V_0}{c} + \alpha\bar{p}\right)(u_i + u_r) = \alpha p(u_i - u_r). \tag{21}$$

As in [6], if we multiply through by $(V_0/c) - \alpha(p + \bar{p})$ and make use of the fact that $\alpha^2 = 1$, we can express u_r in terms of u_i, such that $u_r \equiv r u_i$. We can analogously calculate the adjoint of this equation as $u_r^\dagger = r u_i^\dagger$. Here, r is given by

$$r = \frac{(2V_0/c)((-E/c) + \alpha p)}{(V_0^2/c^2) - (p + \bar{p})^2}. \tag{22}$$

Using the above, one can now calculate the probability current of the reflected wave, which is given by

$$u_r^\dagger u_r = u_i^\dagger r^2 u_i = u_i^\dagger \left(\frac{(2V_0/c)((-E/c) + \alpha p)}{(V_0^2/c^2) - (p + \bar{p})^2}\right)^2 u_i, \tag{23}$$

which can be simplified by using the identity $c u_i^\dagger \alpha u_i = (pc^2/E) u_i^\dagger u_i$ [6], to deduce

$$u_r^\dagger u_r = \left(\frac{2V_0 m_0}{(V_0^2/c^2) - (p + \bar{p})^2}\right)^2 u_i^\dagger u_i \equiv R u_i^\dagger u_i, \tag{24}$$

where R is the reflection coefficient. It is the proportion of particles incident against the barrier that will be reflected. We can assume that $R + T = 1$, where T is the transmission coefficient as we would expect all particles to either be reflected or transmitted. From eq. (24), we can deduce,

$$R = \left(\frac{2V_0 m_0}{(V_0^2/c^2) - (p + \bar{p})^2}\right)^2, \quad \text{and} \quad T = 1 - \left(\frac{2V_0 m_0}{(V_0^2/c^2) - (p + \bar{p})^2}\right)^2. \tag{25}$$

These expressions for R and T allow us to model the Klein paradox. If we consider the case where $V_0 = 0$, we have perfect transmission, which is what we would expect with no barrier. Then we see the reflection coefficient increase as V_0 approaches $E - m_0 c^2$. In fact, $R = 1$ when $V_0 = E - m_0 c^2$ for perfect reflection, but the interesting thing happens for $V_0 > E - m_0 c^2$. We can see implicitly from eq. (25), that if we hold the momenta and masses constant, whilst we increase the potential, the denominator of R will blow up so that R becomes smaller (T becomes larger) and more of the particles will be transmitted through the barrier. We can even see that

if we let V_0 become infinitely large, the reflection coefficient should disappear and we will have perfect transmission. We can quantify this by taking the limit as V_0 goes to infinity in eq. (25), which gives

$$R_{\min} = \lim_{V_0 \to \infty} R(V_0) = \frac{(E/c) - p}{(E/c) + p}, \tag{26}$$

and then we can use the fact that $T_{\max} = 1 - R_{\min}$ to get

$$T_{\max} = \frac{(E/c) + p}{(E/c) + p} - \frac{(E/c) - p}{(E/c) + p} = \frac{2p}{(E/c) + p}. \tag{27}$$

This shows that a large proportion of massive Dirac fermions will penetrate the infinite potential barrier. In the example given in [6], electrons travelling at 80% the speed of light have a transmission coefficient, $T \sim 0.83$. So that 83% of electrons incident on this infinite potential barrier will tunnel through it. In the ultra-relativistic limit, $E >> mc^2$ we see certain penetration through the potential barrier such that $T_{\max} \to 1$ [7]. The final interesting point to note about the general Klein paradox, is that in the massless limit, $E \to pc$, we can see that $T_{\max} = 1$, so that all massless Dirac fermions will penetrate the barrier with certainty.

3.2 The Klein Paradox in Single-Layer Graphene

We have just seen the one-dimensional case for the Klein paradox and we are interested in how the Klein paradox emerges in graphene. The main difference between the general case we have just seen and the graphene case, is that we are now dealing with a two-dimensional system. This leads to the transmission coefficient having an angular dependence [4]. The Klein paradox emerges in graphene when quasiparticle excitations are incident on a potential barrier on the graphene lattice. The quasiparticle excitations turn out to be massless Dirac fermions, so in a one-dimensional case, we would expect perfect transmission always and we will find that this is true in the two-dimensional system when we have normal incidence [7].

In the previous section, we used a one-dimensional Dirac equation (eq. (5)) to derive the Klein paradox. In the case of graphene, we will need it's two-dimensional analogue for a massless spin-half particle [1]. If we take the full Dirac equation (eq. (5)) and set $m = 0$, we get

$$\hat{H}\psi(r) = \alpha_z p_z c \psi(r) = E\psi(r). \tag{28}$$

The 4×4 matrix representation of the α and β matrices given in eq. (6) is only 4×4 because of the β matrix. The algebraic structure of the massive Dirac equation is given by the Clifford algebra, which requires a 4×4 representation [8]. In fact, because we have a massless Dirac equation where the β term has disappeared, we can now use a 2×2 representation as the normal Clifford algebra reduces to $\{\alpha_i, \alpha_j\} = 2\delta_{ij}$ for $i, j = 1, 2, 3$. This algebra can be satisfied by the 2×2 Pauli matrices, σ_i [6]. This means that we can replace α_z with $\boldsymbol{\sigma}$ and we can substitute $p = -i\hbar\partial_z$ to give,

$$-iv_f \boldsymbol{\sigma} \cdot \boldsymbol{\nabla}\psi(r) = E\psi(r), \tag{29}$$

where we have also reduced the speed of light to the fermi velocity, v_f of our quasiparticle on the lattice, which will act as the speed of our light for our massless particle. This is the massless Dirac equation in two dimensions [1], the solutions to which can be given as two-dimensional plane waves analogous to the one-dimensional case.

The Klein paradox in graphene can then be demonstrated using the same method as for the one-dimensional case. We can add together all of the plane wave contributions in the first two regions of fig. 3 and equate them at the region boundaries in order to calculate the proportion of particles penetrating the barrier. The transmission coefficient is then given by

$$T = \frac{\cos^2(\theta)\cos^2(\phi)}{\cos^2(Dq_z)\cos^2(\phi)\cos^2(\theta) + \sin^2(Dq_z)(1 - ss'\sin(\phi)\sin(\theta))^2} \tag{30}$$

as in [1], where $s = \text{sgn}(E)$, $s' = \text{sgn}(E - V_0)$ and $q_z = \sqrt{(V_0 - E)^2/(v_f^2) - k_y^2}$. We also have ϕ and θ as the angles of incidence and transmission, respectively at the boundary between regions *I*, *II* and *III*. In the limit where V_0 goes to infinity, we can see that $ss' = 1(-1)$, which is the case where the Klein paradox arises because we have opposite signs of the energy in regions *I* and *II* [7]. This limit reduces eq. (30) to,

$$T = \frac{\cos^2(\phi)}{1 - \cos^2(q_z D)\sin^2(\phi)}, \tag{31}$$

which makes clear the dependence on the angle of incidence, ϕ [1]. We can see that for normal incidence, $\phi = 0$, that we have perfect transmission. However, we also have perfect transmission regardless of the angle of incidence in the case when $q_z D = n\pi$ for $n \in \mathbb{Z}$. This perfect transmission of massless Dirac fermions on the graphene lattice is an example of the Klein paradox and has been observed experimentally in [9] and [10].

4 The Tight-Binding Model

We have just seen how relativity can lead to real, but unexpected and counter-intuitive physics in graphene. The Klein paradox is only one example of a relativistic effect in a graphene based system. Another relativistic effect that emerges in graphene is the existence of edge states. In order to study these edge states, we will use the tight-binding approximation of a second-quantised Hamiltonian. This allows us to describe a two-dimensional lattice with electron hopping between nearest neighbouring lattice sites. The hopping across the lattice is achieved by using creation and annihilation operators on pairs of lattice sites in a way that annihilates an electron at one site whilst simultaneously creating one at the nearest neighbour site [11]. Firstly, we will find a second-quantised form of a general, quantum mechanical Hamiltonian, before applying the tight-binding approximation to it.

4.1 Second Quantisation

In order to model electron hopping between sites, we need to use a physical theory that allows the number of particles in our system to fluctuate i.e. we want to use creation and annihilation operators to change the particle number. Standard quantum mechanics doesn't allow for a varying number of particles in a system, but once second quantised, it does as it becomes a quantum field theory. From standard quantum mechanics, we know that an electron in a potential is described using the single-particle Schrödinger equation [3]:

$$\hat{H}\left|\psi\right\rangle = \left(\frac{\hat{\boldsymbol{p}}^2}{2m} + V(\boldsymbol{r})\right)\left|\psi\right\rangle = \epsilon\left|\psi\right\rangle, \tag{32}$$

where $\hat{\boldsymbol{p}} = -i\hbar\partial$, ϵ are the eigenvalues of our Hamiltonian operator and $|\psi\rangle$ is the eigenvector in the Hilbert space, $\mathcal{H}$. Our aim is to find a second-quantised version of eq. (32) by using the occupation number representation in a way similar to [11]. We can define a many-body state as $|n_1, n_2, ...\rangle$ where n_i is the number of particles in the ith state, e.g. $|3, 7, ...\rangle$ would mean that there are three particles in the first state and seven in the second. It should be noted, that this example requires that the particles must be bosons, as no two fermions can have the same quantum number due to the Pauli exclusion principle. This state does not exist in the same Hilbert space as its single-particle version, $|\psi\rangle$, but instead exists in a larger Hilbert space that can handle an undetermined number of particles, which is known as a Fock space and is given by

$$\mathcal{F} = \bigoplus_{N=0}^{\infty} \mathcal{H}^N, \tag{33}$$

which is the direct sum of single-particle Hilbert spaces [11]. It includes $\mathcal{H}^0$, which is the space of the one dimensional vacuum state, $|0\rangle$ which is defined in a way such that it can't be acted on by our annihilation operators, which we will go onto define now.

The foundation of our second-quantisation description is the creation and annihilation operators that act as maps within our Fock space. We want to define a creation operator, $a_i^\dagger : \mathcal{F} \mapsto \mathcal{F}$ so that it adds a particle to the ith state number. This can be represented by

$$a_i^\dagger\left|n_1, ..., n_i, ...\right\rangle \equiv (n_i + 1)^{1/2}\zeta^{s_i}\left|n_1, ..., n_i + 1, ...\right\rangle, \quad \forall i \in \mathbb{N}^+ \tag{34}$$

as given in [11]. Here we have ζ^{s_i} to differentiate between the different bosonic and fermionic behaviours and we have $s_i = \sum_{j=1}^{i-1} n_j$. However, the fermionic case won't affect the analysis we are about to perform so we don't need to consider the ζ^{s_i} any further. The term that is raised to the power of a half is a normalisation constant. So we can see that the creation operator acts to add a particle to the n_i particle number in our eigenvector.

We can also define the Hermitian adjoint of our creation operator, we call it the annihilation operator, $a_i = \left(a_i^\dagger\right)^\dagger$ for reasons that will become clear. When we act our annihilation operator

on a state, it behaves according to:

$$a_i \left|n_1, ..., n_i, ...\right\rangle = (n_i)^{1/2} \zeta^{s_i} \left|n_1, ..., n_i - 1, ...\right\rangle, \quad \forall i \in \mathbb{N}^+, \tag{35}$$

which is derivable from eq. (34). It is obvious from this, that the annihilation operator subtracts a particle from the n_ith particle number in our eigenvector. These operators can be used on the vaccum state to generate any N-particle Fock space [11]. The final ingredient we need for the occupation number representation to be of practical use to us is to define the occupation number operator,

$$\hat{n}_{\lambda_i} = a^\dagger_{\lambda_i} a_{\lambda_i} \tag{36}$$

which counts the number of particles in the state λ_i to give $\hat{n}_{\lambda_i} \left|n_{\lambda_1}, n_{\lambda_2}, ...\right\rangle = n_{\lambda_i} \left|n_{\lambda_1}, n_{\lambda_2}, ...\right\rangle$, with n_{λ_i} being the eigenvalue of the operator.

To upgrade a single-particle operator, $\hat{o}$ to its second-quantised version, $\hat{\mathcal{O}}$, we must note that in general, $\hat{\mathcal{O}} = \sum_{n=1}^{N} \hat{o}_n$ for the operator acting on the nth particle [11]. This serves to show that in our many-body system, $\hat{o}_n$ acts on each single-particle state individually and then we can add up all of these contributions to make the many-body operator. We can expect our single-particle operator to behave according to $\hat{o}_{\lambda_i} \left|\lambda_i\right\rangle = o_{\lambda_i} \left|\lambda_i\right\rangle$ where o_{λ_i} is the eigenvalue. However, we must note that in general, we can have multiple particles in the same eigenstate, λ_i and so a more general form of this equation is

$$\hat{o}_{\lambda_i} \left|\lambda_i\right\rangle = n_{\lambda_i} o_{\lambda_i} \left|\lambda_i\right\rangle \tag{37}$$

where as before, n_{λ_i} is the eigenvalue of the number operator. From this, we can see that our many-body operator acts on a state according to,

$$\hat{\mathcal{O}} \left|n_{\lambda_1}, n_{\lambda_2}, ...\right\rangle = \sum_i \hat{o}_{\lambda_i} \left|n_{\lambda_1}, n_{\lambda_2}, ...\right\rangle = \sum_i n_{\lambda_i} o_{\lambda_i} \left|n_{\lambda_1}, n_{\lambda_2}, ...\right\rangle. \tag{38}$$

We can now sandwich our many-body operator between two states in order to derive the relationship between single-particle and many-body operators that we need. Consider

$$\begin{aligned} \left\langle ..., n'_{\lambda_2}, n'_{\lambda_1}\right| \hat{\mathcal{O}} \left|n_{\lambda_1}, n_{\lambda_2}, ...\right\rangle &= \sum_i n_{\lambda_i} o_{\lambda_i} \left\langle ..., n'_{\lambda_2}, n'_{\lambda_1}\right| \left.n_{\lambda_1}, n_{\lambda_2}, ...\right\rangle \\ &= \left\langle ..., n'_{\lambda_2}, n'_{\lambda_1}\right| \sum_i n_{\lambda_i} o_{\lambda_i} \left|n_{\lambda_1}, n_{\lambda_2}, ...\right\rangle \\ &= \left\langle ..., n'_{\lambda_2}, n'_{\lambda_1}\right| \sum_i \hat{n}_{\lambda_i} o_{\lambda_i} \left|n_{\lambda_1}, n_{\lambda_2}, ...\right\rangle. \end{aligned} \tag{39}$$

What we have done here, is make use of eq. (38) in the first line and then moved the sum of the number and operator eigenvalues inside the bra-ket in the second line. We can do this because it is only a number. Between the second and third lines, we swap the number operator eigenvalues for the number operator itself, as this equality holds by definition of the number operator. Now,

using the fact that $\hat{o}\,|\lambda_i\rangle = o\,|\lambda_i\rangle$, which implies that $o_{\lambda_i} = \langle\lambda_i|\,\hat{o}\,|\lambda_i\rangle$, we can deduce,

$$\hat{\mathcal{O}} = \sum_i o_{\lambda_i}\hat{n}_{\lambda_i} = \sum_i \langle\lambda_i|\,\hat{o}\,|\lambda_i\rangle\, a^\dagger_{\lambda_i} a_{\lambda_i}. \tag{40}$$

Finally, we need to swap our diagonal basis, $|\lambda_i\rangle$ for a more general basis which gives,

$$\hat{\mathcal{O}} = \sum_{\mu,\nu} \langle\mu|\,\hat{o}\,|\nu\rangle\, a^\dagger_\mu a_\nu \tag{41}$$

as expressed in [11].

We are finally in a position to derive the many-body version of our Hamiltonian from eq. (32), by using the relations we have derived. When we have $H\,|\psi\rangle = \epsilon_\psi\,|\psi\rangle$, we can rewrite our state using the occupation number representation as $|\psi\rangle = a^\dagger_\psi\,|0\rangle$ and we can infer from eq. (40) that,

$$H = \sum_\psi \epsilon_\psi a^\dagger_\psi a_\psi. \tag{42}$$

We are going to derive the position representation of our Hamiltonian such that $|\boldsymbol{x}\rangle = a^\dagger(\boldsymbol{x})\,|0\rangle$ are the basis states for our N-particle system. We can then use our general basis expression for the second-quantised operator (eq. (41)) to get,

$$H = \int d^d\boldsymbol{x} d^d\boldsymbol{x}' \big\langle \boldsymbol{x}' \big| H \big| \boldsymbol{x} \big\rangle a^\dagger(\boldsymbol{x}') a(\boldsymbol{x}). \tag{43}$$

If we then substitute eq. (32) into the above Hamiltonian we get,

$$H = \int d^d\boldsymbol{x} d^d\boldsymbol{x}' \big\langle \boldsymbol{x}' \big| \left(\frac{\hat{\boldsymbol{p}}^2}{2m} + V \right) \big| \boldsymbol{x} \big\rangle a^\dagger(\boldsymbol{x}') a(\boldsymbol{x}). \tag{44}$$

which we can simplify by multiplying out the brackets and sandwiching $\hat{\boldsymbol{p}}$ and V inside the bra-kets. We make use of the following relations,

$$\big\langle \boldsymbol{x}' \big| V(\boldsymbol{x}) \big| \boldsymbol{x} \big\rangle = V(\boldsymbol{x})\delta^d(\boldsymbol{x} - \boldsymbol{x}'), \quad \big\langle \boldsymbol{x}' \big| \hat{\boldsymbol{p}}^2 \big| \boldsymbol{x} \big\rangle = -\hbar^2\partial^2\delta^d(\boldsymbol{x} - \boldsymbol{x}') \tag{45}$$

where the d-dimensional delta functions serve to force $\boldsymbol{x}' \mapsto \boldsymbol{x}$. This gives

$$H = \int d^d\boldsymbol{x}\; a^\dagger(\boldsymbol{x}) \left(\frac{\hat{\boldsymbol{p}}^2}{2m} + V \right) a(\boldsymbol{x}) \tag{46}$$

which is the final version of our second-quantised Hamiltonian on an N-dimensional many-body system.

4.2 The Tight-Binding Hamiltonian for Graphene

The tight-binding model relies on considering a system that is made out of nearly-isolated atoms. By this, we mean that the atoms are far enough apart that inter-atomic interactions are very small but the valence band electrons have slightly overlapping wavefunctions [12]. This gives us a model where the electrons are "tightly bound" to their parent atoms but with a small chance of hopping to nearest-neighbour atomic sites. This approximation is valid in regimes where the inter-atomic spacing is larger than the radius of the valence band orbitals, but not so large that we have a system of completely isolated atoms. With the distance between two nearest-neighbour carbon atoms in graphene being $a \approx 1.42$Å, the tight-binding model is the appropriate choice of model for graphene [1]. It should be noted that in the following derivation, we will ignore the effects of spin, as it will not be important in our analysis of edge states in carbon nanotubes.

In order to find a tight-binding Hamiltonian of graphene, we must make use of an important result from condensed matter physics relating to periodic potentials: Bloch's Theorem. This theorem states that when we have a periodic potential of the form $V(\boldsymbol{r}+\boldsymbol{R}) = V(\boldsymbol{r})$ for all $\boldsymbol{R}$ in a Bravais lattice, then the wavefunctions ψ of a one-electron Hamiltonian can be given in the form

$$\psi_{n\boldsymbol{k}}(\boldsymbol{r}) = e^{i\boldsymbol{k}\cdot\boldsymbol{r}} u_{n\boldsymbol{k}}(\boldsymbol{r}), \tag{47}$$

which is a plane wave multiplied by a function, $u_{n\boldsymbol{k}}$ known as the Bloch function that is periodic on the lattice according to

$$u_{n\boldsymbol{k}}(\boldsymbol{r}+\boldsymbol{R}) = u_{n\boldsymbol{k}}(\boldsymbol{r}). \tag{48}$$

What this means is that the wavefunctions of the one-electron Hamiltonian can be thought of as periodic, up to some plane wave factor. This is more obvious from the alternative statement of Bloch's Theorem:

$$|\psi(\boldsymbol{r}+\boldsymbol{R})\rangle = e^{i\boldsymbol{k}\cdot\boldsymbol{R}} |\psi(\boldsymbol{r})\rangle , \tag{49}$$

for every $\boldsymbol{R}$ in the Bravais lattice [12].

We also need to decide which basis states we want to use to describe our system. Ideally, we want an orthonormal basis to make our analysis easier. The best basis for a tight-binding approximation involves the use of Wannier functions as they are maximally localised and form a complete, orthonormal basis. This means that they are ideal for systems in the limit where we are getting close to having isolated atoms, whilst still allowing for some inter-atomic interactions, as is the case with graphene. The Wannier states are defined to be the Fourier transform of the Bloch functions, $|\psi_{n\boldsymbol{k}}\rangle$, which carries over the property of orthogonality from the Bloch functions [13]. So the Wannier function are defined by the following transformations,

$$|\psi_{n\boldsymbol{R}}\rangle = \frac{1}{\sqrt{N}} \sum_{\boldsymbol{k}}^{B.Z.} e^{-i\boldsymbol{k}\cdot\boldsymbol{R}} |\psi_{n\boldsymbol{k}}\rangle , \quad |\psi_{n\boldsymbol{k}}\rangle = \frac{1}{\sqrt{N}} \sum_{\boldsymbol{R}} e^{i\boldsymbol{k}\cdot\boldsymbol{R}} |\psi_{n\boldsymbol{R}}\rangle , \tag{50}$$

where $\sum_{\boldsymbol{k}}^{B.Z.}$ is a sum over all $\boldsymbol{k}$ in the first Brillouin zone [11].

Our aim from this point on is to use Bloch's Theorem and the Wannier states to derive a tight-binding Hamiltonian that we can use for graphene. Firstly, we can use the Wannier states to define transformations for our creation and annihilation operators. If we fix the band so that we can remove the n index, begin using the index $i = 1, ..., N$ which enumerates the lattice sites $\boldsymbol{R}_i$, and make use of the fact that the single-particle state $|\psi_i\rangle = a_i^\dagger |0\rangle$, then we can deduce from the definition of the Wannier functions that our creation operators can be expressed as

$$a_i^\dagger = \frac{1}{\sqrt{N}} \sum_{\boldsymbol{k}}^{B.Z.} e^{-i\boldsymbol{k}\cdot\boldsymbol{R}_i} a_{\boldsymbol{k}}^\dagger, \quad a_{\boldsymbol{k}}^\dagger = \frac{1}{\sqrt{N}} \sum_i e^{i\boldsymbol{k}\cdot\boldsymbol{R}_i} a_i^\dagger, \tag{51}$$

where similar expressions for the annihilation operators can be derived in the same way.

Now, if we make use of the fact that the Bloch states diagonalise a single-particle Hamiltonian [11], then we can use eq. (42) and substitute in the operator transformation above to give

$$\begin{aligned} H &= \sum_{\boldsymbol{k}} \epsilon_{\boldsymbol{k}} a_{\boldsymbol{k}}^\dagger a_{\boldsymbol{k}}, \\ &= \sum_{\boldsymbol{k}} \epsilon_{\boldsymbol{k}} \left(\frac{1}{\sqrt{N}} \sum_i e^{i\boldsymbol{k}\cdot\boldsymbol{R}_i} a_i^\dagger \right) \left(\frac{1}{\sqrt{N}} \sum_{i'} e^{-i\boldsymbol{k}\cdot\boldsymbol{R}_{i'}} a_{i'} \right), \\ &= \frac{1}{N} \sum_{\boldsymbol{k}} \sum_{ii'} e^{i\boldsymbol{k}\cdot(\boldsymbol{R}_i - \boldsymbol{R}_{i'})} \epsilon_{\boldsymbol{k}} a_i^\dagger a_{i'}. \end{aligned} \tag{52}$$

We can understand this expression by looking at the creator and annihilation operator in the last line. We can interpret this as creating a particle at the site $\boldsymbol{R}_i$ and annihilating one at site $\boldsymbol{R}_{i'}$, which simulates the hopping of a particle between the sites. The normalisation and $\boldsymbol{k}$-dependent terms of the expression can be interpreted as the coupling strength that determines the probability of the hopping between sites. In order to tidy up this expression, we can define the coupling strength to be the matrix hopping element, $t_{ii'}$ such that

$$H \equiv \sum_{ii'} a_i^\dagger t_{ii'} a_{i'}, \tag{53}$$

where $t_{ii'} = N^{-1} \sum_{\boldsymbol{k}} e^{i\boldsymbol{k}\cdot(\boldsymbol{R}_i - \boldsymbol{R}_{i'})} \epsilon_{\boldsymbol{k}}$ is the coupling strength for a hopping from the $\boldsymbol{R}_{i'}$ site to $\boldsymbol{R}_i$. For completeness, we should also include the ability to reverse this process by hopping from the $\boldsymbol{R}_i$ site to the $\boldsymbol{R}_{i'}$ one. We do this by including the Hermitian conjugate in the tight-binding Hamiltonian

$$H = \sum_{ii'} (a_i^\dagger t_{ii'} a_{i'} + a_{i'}^\dagger t_{i'i} a_i) = \sum_{ii'} (a_i^\dagger t_{ii'} a_{i'} + \text{h.c.}), \tag{54}$$

which is the general form of the tight-binding Hamiltonian, where h.c. is the Hermitian conjugate.

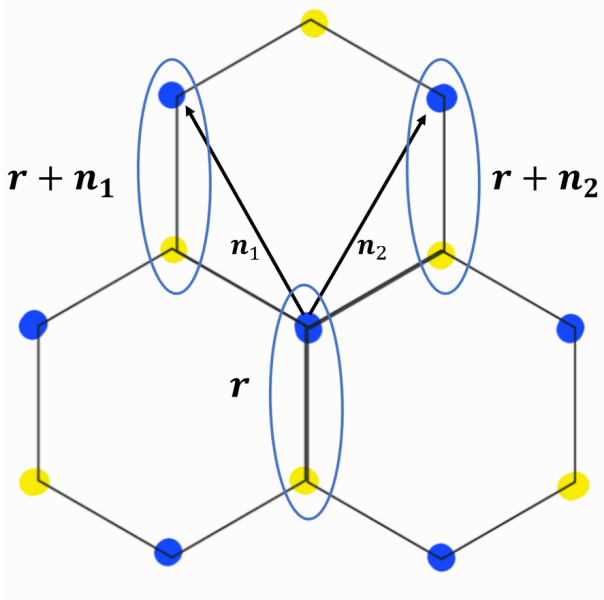

Figure 4: The nearest-neighbour hopping from any site to another must always be between the two sub-lattices. That is to say, if we begin on the A sub-lattice, any nearest neighbour hopping will take us to the B sub-lattice. There are three possible hoppings from any site. If we consider starting on the blue site in the centre of the figure, then we can hop downwards within the same unit cell, or diagonally to the nearest neighbours in other unit cells, which leads to the Hamiltonian given in eq. (56).

In order to use eq. (54) as a Hamiltonian for graphene, there are a few things we need to note. Firstly, as shown in fig. 2, our system is actually made up of two triangular sub-lattices, A and B, where all the nearest neighbours of each site are part of the the other sub-lattice. This means that all nearest-neighbour interactions happen between sub-lattices A and B. As such, we will restrict $a_i^\dagger$ and a_i to act on the A sub-lattice and introduce $b_i^\dagger$ and b_i to act on the B sub-lattice. This means our Hamiltonian in eq. (54) can be re-written as

$$H = -t \sum_{ii'} (a_i^\dagger b_{i'} + \text{h.c.}), \tag{55}$$

where we have also made the choice to set $t_{ii'} = -t$. We can do this because we are assuming that our system is symmetric under translation, and therefore the coupling strength is constant for all nearest-neighbour links.

Finally, we will bring our Hamiltonian into its appropriate form by changing the summation index and considering the possible translations on the lattice. In eq. (55), we sum over all i and i' sites for nearest neighbour pairs. Instead, what we can do is sum over all the position vectors in the A sub-lattice, $\boldsymbol{r} \in A$. By looking at fig. 4, we can now expand eq. (55) in terms of the three possible nearest-neighbour hoppings, which are given by the translated position vectors $\boldsymbol{r}$, $\boldsymbol{r}+\boldsymbol{n}_1$ and $\boldsymbol{r}+\boldsymbol{n}_2$. This means we can define corresponding creation operators $b_{\boldsymbol{r}}$, $b_{\boldsymbol{r}+\boldsymbol{n}_1}$ and $b_{\boldsymbol{r}+\boldsymbol{n}_2}$, that will act to create a particle on the nearest-neighbour site when our annihilation

operator destroys one at the central site. This gives our Hamiltonian in the form

$$H = -t \sum_{\boldsymbol{r} \in A} a^\dagger_{\boldsymbol{r}} (b_{\boldsymbol{r}} + b_{\boldsymbol{r}+\boldsymbol{n_1}} + b_{\boldsymbol{r}+\boldsymbol{n_2}}) + \text{h.c.} \tag{56}$$

which is the primary form of the tight-binding Hamiltonian for graphene that we will use in our analysis.

5 The Dispersion Relation for Graphene

If we are going to use eq. (56) to describe carbon nanotubes, we want to rewrite it in terms of matrices and find it's associated dispersion relation. This will make our analysis easier when we come to Taylor expand our Hamiltonian about the Dirac points so that we can isolate the relativistic phenomena in the system.

We define creation and annihilation operators for our system like before, in terms of their Fourier transforms

$$\begin{aligned} a_{\boldsymbol{r}} = \frac{1}{\sqrt{N}} \sum_{\boldsymbol{p}}^{B.Z.} e^{i\boldsymbol{p}\cdot\boldsymbol{r}} a_{\boldsymbol{p}} \quad &\Longrightarrow \quad a^\dagger_{\boldsymbol{r}} = \frac{1}{\sqrt{N}} \sum_{\boldsymbol{p}}^{B.Z.} e^{-i\boldsymbol{p}\cdot\boldsymbol{r}} a^\dagger_{\boldsymbol{p}}, \\ b_{\boldsymbol{r}} = \frac{1}{\sqrt{N}} \sum_{\boldsymbol{q}}^{B.Z.} e^{i\boldsymbol{q}\cdot\boldsymbol{r}} b_{\boldsymbol{q}} \quad &\Longrightarrow \quad b^\dagger_{\boldsymbol{r}} = \frac{1}{\sqrt{N}} \sum_{\boldsymbol{q}}^{B.Z.} e^{-i\boldsymbol{q}\cdot\boldsymbol{r}} b^\dagger_{\boldsymbol{q}}, \end{aligned} \tag{57}$$

where a and b act on the A and B sub-lattices respectively, as do $\boldsymbol{p}$ and $\boldsymbol{q}$. We can now substitute these into eq. (56) to get

$$\begin{aligned} H &= -\frac{t}{N} \sum_{\boldsymbol{r} \in A} \sum_{\boldsymbol{p}}^{B.Z.} \sum_{\boldsymbol{q}}^{B.Z.} e^{-i\boldsymbol{p}\cdot\boldsymbol{r}} a^\dagger_{\boldsymbol{p}} \Big(e^{i\boldsymbol{q}\cdot\boldsymbol{r}} + e^{i\boldsymbol{q}\cdot(\boldsymbol{r}+\boldsymbol{n_1})} + e^{i\boldsymbol{q}\cdot(\boldsymbol{r}+\boldsymbol{n_2})} \Big) b_{\boldsymbol{q}} + \text{h.c.} \\ &= -t \sum_{\boldsymbol{p}}^{B.Z.} \sum_{\boldsymbol{q}}^{B.Z.} a^\dagger_{\boldsymbol{p}} b_{\boldsymbol{q}} \big(1 + e^{i\boldsymbol{q}\cdot\boldsymbol{n_1}} + e^{i\boldsymbol{q}\cdot\boldsymbol{n_2}} \big) \left(\frac{1}{N} \sum_{\boldsymbol{r} \in A} e^{-i(\boldsymbol{p}-\boldsymbol{q})\cdot\boldsymbol{r}} \right) + \text{h.c.} \end{aligned} \tag{58}$$

where $N^{-1} \sum_{\boldsymbol{r} \in A} e^{-i(\boldsymbol{p}-\boldsymbol{q})\cdot\boldsymbol{r}} = \delta_{\boldsymbol{p}\boldsymbol{q}}$ as we are summing over the roots of unity. This leaves us with a simplified version of our Hamiltonian given by

$$H = \sum_{\boldsymbol{p}}^{B.Z.} \Big(f(\boldsymbol{p}) a^\dagger_{\boldsymbol{p}} b_{\boldsymbol{p}} + f^*(\boldsymbol{p}) b^\dagger_{\boldsymbol{p}} a_{\boldsymbol{p}} \Big), \tag{59}$$

where we define $f(\boldsymbol{p}) = -t(1 + e^{i\boldsymbol{p}\cdot\boldsymbol{n}_1} + e^{i\boldsymbol{p}\cdot\boldsymbol{n}_2})$. It can be seen from the above expression that H can be expressed in terms of matrices. This matrix representation of our Hamiltonian is

$$H = \sum_{\boldsymbol{p}}^{B.Z.} \begin{pmatrix} a^\dagger_{\boldsymbol{p}} & b^\dagger_{\boldsymbol{p}} \end{pmatrix} \begin{pmatrix} 0 & f(\boldsymbol{p}) \\ f^*(\boldsymbol{p}) & 0 \end{pmatrix} \begin{pmatrix} a_{\boldsymbol{p}} \\ b_{\boldsymbol{p}} \end{pmatrix}. \tag{60}$$

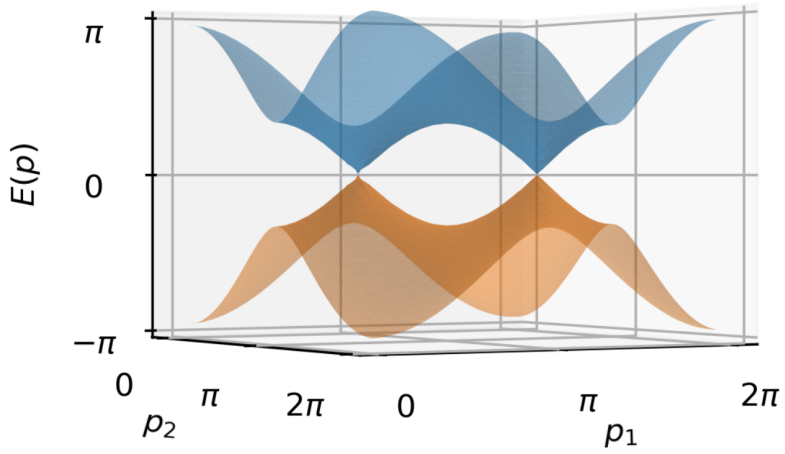

Figure 5: The dispersion relation for graphene (eq. (65)) with the two Dirac points visible at $E(\boldsymbol{p}) = 0$. From this figure, the Dirac cones in the low-energy sector are clearly visible in the direct vicinity of the Dirac points.

Finally, if we define $\psi_{\boldsymbol{p}} = (a_{\boldsymbol{p}}, b_{\boldsymbol{p}})^T$, then we have

$$H = \sum_{\boldsymbol{p}}^{\mathrm{BZ}} \psi_{\boldsymbol{p}}^\dagger h(\boldsymbol{p}) \psi_{\boldsymbol{p}}, \quad h(\boldsymbol{p}) = \begin{pmatrix} 0 & f(\boldsymbol{p}) \\ f^*(\boldsymbol{p}) & 0 \end{pmatrix}, \tag{61}$$

where $h(\boldsymbol{p})$ is the single-particle Hamiltonian. By solving the characteristic polynomial of $h(\boldsymbol{p})$, we find the eigenenergies are $E(\boldsymbol{p}) = \pm|f(\boldsymbol{p})|$.

Our expression for $f(\boldsymbol{p})$ can be expanded in terms of the reciprocal basis given in eq. (4). By making use of Bloch's theorem and the discrete, translational symmetry of our lattice, we know that the crystal momentum will be periodic. We can express this periodicity as $N_i \boldsymbol{p} \cdot \boldsymbol{n}_i = 2\pi m_i$, where $m_i \in \mathbb{Z}$, and $i = 1, 2$ denotes our basis vectors. This leads to our quantised crystal momentum, which expanded in the reciprocal basis is given by

$$\boldsymbol{p} = \frac{a}{2\pi} \sum_i p_i \boldsymbol{G}_i = \frac{a}{2\pi} \big(p_1 \boldsymbol{G}_1 + p_2 \boldsymbol{G}_2\big), \tag{62}$$

where a is the lattice constant. By substituting this expression for the momentum into $f(\boldsymbol{p})$ and making use of the fact that $\boldsymbol{G}_i \cdot \boldsymbol{n}_j = 2\pi\delta_{ij}$, we get

$$\begin{aligned} f(\boldsymbol{p}) &= -t\Big(1 + e^{i\frac{a}{2\pi}(p_1\boldsymbol{G}_1 + p_2\boldsymbol{G}_2)\cdot\boldsymbol{n}_1} + e^{i\frac{a}{2\pi}(p_1\boldsymbol{G}_1 + p_2\boldsymbol{G}_2)\cdot\boldsymbol{n}_2}\Big), \\ &= -t\Big(1 + e^{i\frac{a}{2\pi}p_1\boldsymbol{G}_1\cdot\boldsymbol{n}_1} + e^{i\frac{a}{2\pi}p_2\boldsymbol{G}_2\cdot\boldsymbol{n}_2}\Big), \\ &= -t\big(1 + e^{iap_1} + e^{iap_2}\big). \end{aligned} \tag{63}$$

We can now find an expression for $E(\boldsymbol{p})$ in terms of p_1 and p_2 by first considering

$$|f(\boldsymbol{p})|^2 = f(\boldsymbol{p})f^*(\boldsymbol{p}) = t^2\Big(3 + e^{-iap_1} + e^{-iap_2} + e^{iap_1} + e^{ia(p_1-p_2)} + e^{iap_2} + e^{ia(p_2-p_1)}\Big). \quad (64)$$

This can be simplified by using Euler's formula in the form $e^{iap_j} = \cos(ap_j) + i\sin(ap_j)$ for $j = 1, 2$. By substituting in Euler's formula and simplifying, we arrive at the dispersion relation for graphene,

$$E(\boldsymbol{p}) = \pm|f(\boldsymbol{p})| = \pm t\sqrt{3 + 2\cos(ap_1) + 2\cos(ap_2) + 2\cos(a(p_1 - p_2))}, \quad (65)$$

which is shown in fig. 5.

6 Review of Edge States in Zigzag Carbon Nanotubes

We are now in a position to consider the existence of edge states in graphene based systems. These can take the form of zero modes, that exist at the edge of graphene flakes [14] or carbon nanotubes [15]. These states are energy eigenstates localised at the edge with zero energy [7]. However, these are not the edge states we will be concerned with in this thesis. It turns out that in carbon nanotubes with zigzag ends, there is theoretical support for bulk states at the ends of the tube [2]. This section will summarise the results of [2], so that we can perform an analogous analysis of carbon nanotubes with armchair edges in the remainder of this thesis.

6.1 Zigzag Momentum Quantisation and Dispersion Relation

In order to build a carbon nanotube, we must apply another set of periodic boundary conditions to the system of graphene that we've been working with so far. The first set of periodic boundary conditions were applied when we used Bloch's Theorem to understand the translational symmetry of the graphene lattice in eq. (49). Referring to fig. 2, if we impose periodic boundary conditions in the x-direction, it will create a nanotube with zigzag edges. Suppose the circumference of the nanotube is given by Na, where N is the number of unit cells in the x-direction and a is the lattice constant, as it was before. We can construct an infinitely long nanotube by letting the length of the nanotube L, tend to infinity in the y-direction as we take the thermodynamic limit. This leads to a momentum quantisation of the kind where the p_2 component remains unconstrained, but with

$$p_1 = \frac{2n\pi}{Na}, \quad (66)$$

in the first Brillouin zone [2].

For graphene, the dispersion relation is between the unconstrained momentum $\boldsymbol{p} = (p_1, p_2)$, and the energy $E(\boldsymbol{p})$. Now we have quantised p_1, we have reduced our dispersion relation into one-dimensional bands enumerated by the integer n. We are essentially taking slices of the

dispersion relation in fig. 5, for each quantised value of the momentum. We want to substitute our expression for p_1 into the dispersion relation of graphene (eq. (65)). This gives us a zigzag dispersion relation given by

$$E_n(k) = \pm t\sqrt{3 + 2\cos\left(\frac{2n\pi}{N}\right) + 2\cos\left(\frac{2n\pi}{N} - ka\right) + 2\cos(ka)}, \tag{67}$$

where $p_2 \to k$. It should be noted that $E_n(k)$ has a single minima for each value of n. It is at the low-energy limit of these bands where we find the cones of $E \sim k$. These cones are centred at the two zero energy Dirac points in the Brillouin zone. In order to focus on these low-energy properties, we want to take th continuum limit by Taylor expanding about the minima of the dispersion, as this will allow us to ignore the non-linear terms of the momentum. Therefore, we will be considering the properties of the conic section of the Brillouin zone where the relativistic energy-momentum relation is obeyed.

In order to find the minima of the dispersion, we differentiate $E_n^2(k)$, rather than $E_n(k)$ as it is easier to work with. The square of the energy will have the same minima as the energy, therefore we can set it's derivative equal to zero in order to find the turning points of the bands at $k_{\min}$. This gives us the equation

$$\left(E_n^2(k)\right)' = 2t^2 a\left(\sin\left(\frac{2n\pi}{N} - ka\right) - \sin(ka)\right) = 0, \tag{68}$$

which implies that

$$\sin\left(\frac{2n\pi}{N} - k_{\min}a\right) = \sin(k_{\min}a). \tag{69}$$

We can now make use of the fact that $\sin(x) = \sin(y)$ implies that $x = m\pi + (-1)^m y$ for $m \in \mathbb{Z}$, to obtain

$$k_{\min} = \left(\frac{2n}{N} - m\right)\frac{\pi}{a(1 + (-1)^m)}, \quad m \in \mathbb{Z}. \tag{70}$$

In order to stop the denominator outside of the brackets from being zero, we require m to be even, so we set $m = -2l$ to give

$$k_{\min} = \left(\frac{n}{N} + l\right)\frac{\pi}{a} \qquad \mod \frac{2\pi}{a}, \quad l \in \mathbb{Z}. \tag{71}$$

By considering the constraint that $k_{\min}$ is modulo $2\pi/a$, and the fact that $n/N \in [0, 1]$, the only possibilities for l are that $l = 0, 1$. We want to deduce which of these turning points is the minima. We do this by calculating $\left(E_n^2(k)\right)''$ and seeing for which turning points is greater than zero. This leads to

$$k_{\min}^n = \begin{cases} \frac{\pi}{a}\left(\frac{n}{N}\right) & \text{if } n > \frac{N}{2}, \\ \frac{\pi}{a}\left(\frac{n}{N} + 1\right) & \text{if } n < \frac{N}{2}. \end{cases} \tag{72}$$

The case where $n = N/2$ does not have a minima as it is a flat band [2]. As we are only interested in the low-energy properties of the nanotube, we will focus on the lower momentum eigenstates where $n < N/2$. This means we have a final expression for our band minima, given by

$$k^n_{\min} = \frac{\pi}{a}\left(\frac{n}{N} + 1\right). \tag{73}$$

6.2 Support of Bulk States at the Edge

Now that we have the minima of our bands, we need to Taylor expand the Hamiltonian about these minima to linear order in the momentum. The Hamiltonian (eq. (61)) can expanded out in terms of its Taylor series about $k^n_{\min}$, we do this by using

$$f_n(k^n_{\min} + p) = f_n(k^n_{\min}) + pf'_n(k^n_{\min}) + \mathcal{O}(p^2), \tag{74}$$

such that

$$h(\boldsymbol{p}) = \begin{pmatrix} 0 & f_n(k^n_{\min} + p) \\ f^*_n(k^n_{\min} + p) & 0 \end{pmatrix}, \tag{75}$$

according to [2]. After substituting $k^n_{\min}$ (eq. (73)) into $f(\boldsymbol{p})$ (eq. (63)), we arrive at the continuum limit Hamiltonian,

$$h(\boldsymbol{p}) = \begin{pmatrix} 0 & e^{i\frac{n\pi}{N}}(\Delta_n + iatp) \\ e^{-i\frac{n\pi}{N}}(\Delta_n - iatp) & 0 \end{pmatrix} + \mathcal{O}(p^2), \tag{76}$$

where Δ_n is an effective mass of the system which represents band gaps in the dispersion. It turns out that the system is gapless ($|\Delta_n| = 0$) when $n/N = 1/3$ for $n, N \in \mathbb{Z}$, which means that N must be a multiple of 3 for this to occur. The single particle Hamiltonian above is a (1+1) dimensional massive Dirac Hamiltonian where $\alpha^x = \sigma^y$ and $\beta = \sigma^x$ [2]. We can use this Hamiltonian to build suitable Dirac wavefunctions for our system. According to [2], this gives us the Dirac equation in the form

$$\begin{pmatrix} 0 & e^{i\frac{n\pi}{N}}(\Delta_n + iatp) \\ e^{-i\frac{n\pi}{N}}(\Delta_n - iatp) & 0 \end{pmatrix} \begin{pmatrix} \psi_A \\ \psi_B \end{pmatrix} = E_n(p) \begin{pmatrix} \psi_A \\ \psi_B \end{pmatrix}, \tag{77}$$

where ψ_A and ψ_B can be interpreted as the wavefunctions of the A and B triangular sub-lattices, respectively. The wavefunctions can then be found to be of the form

$$\psi_{n,p} = \frac{1}{\sqrt{2}} \begin{pmatrix} 1 \\ se^{-in\pi/N} e^{i\theta_{n,p}} \end{pmatrix} e^{ipx}, \tag{78}$$

where $s = \text{sgn}(E_n)$ and $\theta_{n,p} = \arg(\Delta_n + iatp)$ is an angle in the complex plane. Using the above, we can build a superposition out of forward and backward propagating standing waves,

$$\psi_{n,p} = \begin{pmatrix} 1 \\ e^{-in\pi/N} e^{-i\theta_{n,p}} \end{pmatrix} e^{ipx} + R \begin{pmatrix} 1 \\ e^{-in\pi/N} e^{i\theta_{n,p}} \end{pmatrix} e^{-ipx}, \quad R \in \mathbb{C}. \tag{79}$$

All that needs to be done is apply the zigzag boundary conditions to our standing waves and see what we are left with. The boundary conditions for the zigzag edge are given by

$$\psi_A(0) = \psi_B(L) = 0 \tag{80}$$

for the continuum limit approximation of a carbon nanotube of length L [1][2]. These boundary conditions are not as simple as the non-relativistic case where for a particle obeying the Schrödinger equation, we just require the wavefunction to be zero at the boundary. In fact, eq. (80) are a special case of the more general rule for Dirac boundary conditions, which requires the Dirac current normal to the boundary to be zero. This different rule for the boundary conditions is due to the fact that in certain situations, requiring the wavefunction to be zero at the boundary would make a Dirac spinor zero everywhere, which is unhelpful in understanding physical situations [2]. This requirement on the current, rather than the value of the spinor at the edge of the system, is what allows the spinor in certain situations, to give rise to a non-zero density at the edge. We will now see an example of how this manifests itself for a zigzag carbon nanotube.

By applying the boundary conditions of eq. (80) to eq. (79), the final solution of the wavefunction for a finite, zigzag carbon nanotube is given by

$$\psi_{n,p} = \mathcal{N}_{n,p} \begin{pmatrix} \sin(px) \\ e^{-in\pi/N} \sin(px - \theta_{n,p}) \end{pmatrix}, \tag{81}$$

in position space, where $\mathcal{N}$ is some normalisation constant [2]. The second equality of the boundary conditions means that we require $pL - \theta_{n,p} = m\pi$ for $m \in \mathbb{Z}$. If we continue to interpret the upper component of the spinor as the A sub-lattice and the bottom one as the B sub-lattice, then we can see that $\theta_{n,p}$ acts as a phase difference between the wavefunctions of the two triangular sub-lattices.

By using the definition of the charge density, we can see that

$$\rho_{n,p} = \psi^\dagger_{n,p} \psi_{n,p} = |\mathcal{N}|^2 \Big(\sin^2(px) + \sin^2(px + \theta_{n,p}) \Big). \tag{82}$$

which is understood to be the sum of the charge densities of the sub-lattices A and B, such that $\rho = \psi^\dagger \psi = |\psi_A|^2 + |\psi_B|^2$. We can see from the above equation that the density is not necessarily

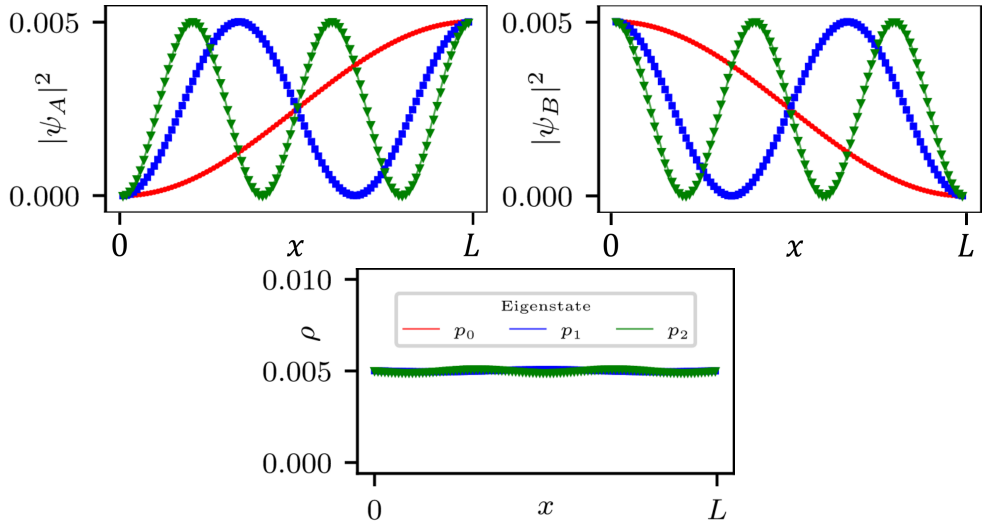

Figure 6: Numerical simulation of a zigzag carbon nanotube taken from [2]. The three colours represent the first three eigenstates of the system, where red is the ground state, blue is the first excitation and green is the second. Top row: the left and right plots show the charge density of the A and B sub-lattice respectively, which can be interpreted as the top and bottom components of the spinor in eq. (81). The density is plotted against the length of the system, $0 < x < L$. We see that for each sub-lattice, there is a non-zero density at one of the edges. Bottom row: we plot the overall charge density, $\rho = |\psi_A|^2 + |\psi_B|^2$ which is non-zero at both edges. This plot corresponds to and agrees with eq. (82).

zero at the edges of the carbon nanotube,

$$\rho_{n,p}(0) = \rho_{n,p}(L) = |\mathcal{N}|^2 \sin^2(\theta_{n,p}), \tag{83}$$

which is maximised for $\theta_{n,p} = \arg(\Delta_n + iatp) = \pi/2$. This condition for the maxima suggests that the edge density of the nanotube is maximised for a gapless system ($\Delta_n = 0$), as this would correspond to the $\pi/2$ rotation in the complex plane. Therefore, as we know the gapless band only occur when $n/N = 1/3$, this is also the condition that maximises the edge density. The maximum edge density is not dependent on the momentum of the system and is given by $\rho_n = |\mathcal{N}|^2 = 1/L$. According to [2], the density at the edge becomes vanishingly small when a gap is opened in the dispersion. These results are all supported by numerical simulations [2], which is demonstrated in fig. 6.

7 Analysis of Armchair Carbon Nanotubes

Now that we have reviewed the existence of edge states in zigzag carbon nanotubes, we will perform a similar analysis on a nanotube with armchair edges and compare the results. In this section, we will follow the same process as we outlined for zigzag carbon nanotubes.

7.1 Armchair Momentum Quantisation and Dispersion Relation

As in the previous section, the first step is to apply a periodicity to the momentum, along the circumference of the edge. For the zigzag case, we chose the boundary to go along the $\boldsymbol{n}_1$ direction in fig. 2. For the armchair case, we need to use a slightly more complicated choice and use the $\boldsymbol{n}_1 + \boldsymbol{n}_2$ direction. We then use Bloch's Theorem (eq. (49)) to derive the necessary quantisation condition for our momenta. If we consider a unitary translation operator acting on our momentum eigenstates $|\boldsymbol{p}\rangle$,

$$T(\boldsymbol{r})\,|\boldsymbol{p}\rangle = e^{i\boldsymbol{p}\cdot\boldsymbol{r}}\,|\boldsymbol{p}\rangle\,, \tag{84}$$

then we can substitute our armchair momentum vector for $\boldsymbol{r}$, to give

$$T(\boldsymbol{n}_1 + \boldsymbol{n}_2)\,|\boldsymbol{p}\rangle = e^{i\boldsymbol{p}\cdot(\boldsymbol{n}_1+\boldsymbol{n}_2)}\,|\boldsymbol{p}\rangle\,. \tag{85}$$

We note that for a carbon nanotube with circumference of length Na, that

$$T(N(\boldsymbol{n}_1 + \boldsymbol{n}_2))\,|\boldsymbol{p}\rangle = e^{iN\boldsymbol{p}\cdot(\boldsymbol{n}_1+\boldsymbol{n}_2)}\,|\boldsymbol{p}\rangle = |\boldsymbol{p}\rangle\,, \tag{86}$$

because we move around the edge N times and arrive back at our starting position. This implies that $N\boldsymbol{p}\cdot(\boldsymbol{n}_1+\boldsymbol{n}_2) = 2\pi n$ for $n \in \mathbb{Z}$. By substituting in our expression for $\boldsymbol{p}$ as given in eq. (62) and using $\boldsymbol{G}_i \cdot \boldsymbol{n}_j = 2\pi\delta_{ij}$ to simplify, we arrive at the armchair momentum quantisation where

$$p_1 + p_2 = \frac{2\pi n}{Na}. \tag{87}$$

This means that just like in the zigzag case, we have quantised momenta around the circumference of the nanotube in the $\boldsymbol{n}_1 + \boldsymbol{n}_2$ direction, but unconstrained momenta along the length of the nanotube in the $\boldsymbol{n}_1 - \boldsymbol{n}_2$ direction.

Our quantised momenta can now be substituted into the graphene dispersion relation (eq. (65)) in order to get

$$E_n(k) = \pm t\sqrt{3 + 2\cos\left(\left(\frac{2n\pi}{Na} - k\right)a\right) + 2\cos\left(\left(\frac{2n\pi}{Na} - 2k\right)a\right) + 2\cos(ka)}, \tag{88}$$

which is shown in fig. 7. As before, we need to find the minima of this dispersion for the lower energy bands in order to focus in on the relativistic phenomena. We will work with $E_n^2(k)$ again as it has the same turning points as the dispersion relation. We have

$$E_n^2(k) = t^2\left(3 + 2\cos\left(\left(\frac{2\pi n}{Na} - k\right)a\right) + 2\cos\left(\left(\frac{2\pi n}{Na} - 2k\right)a\right) + 2\cos(ka)\right), \tag{89}$$

which can be differentiated and set to zero to give the turning points,

$$\left(E_n^2(k_{\min})\right)' = 2t^2\left[a\sin\left(\left(\frac{2\pi n}{Na} - k_{\min}\right)a\right) + 2\sin\left(\left(\frac{2\pi n}{Na} - 2k_{\min}\right)a\right) - \sin(k_{\min}a)\right] = 0, \tag{90}$$

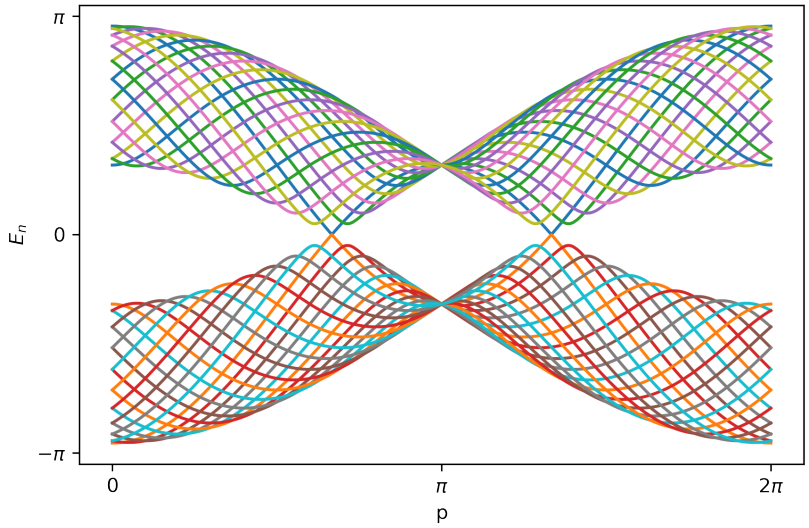

Figure 7: The dispersion relation for a carbon nanotube with armchair edges (eq. (88)). This is a numerical simulation of the first 20 energy bands $E_n(p)$ of the system. In this simulation, $t = a = 1$ and the nanotube circumference is determined by $N = 20$.

which can be reduced to

$$\sin\left(\frac{\pi n}{N} - k_{\min}a\right)\left[2\cos\left(\frac{\pi n}{N} - k_{\min}a\right) + \cos\left(\frac{\pi n}{N}\right)\right] = 0. \tag{91}$$

Either the sin function or the contents of the square brackets must equal zero. If we set the sin function to be zero, we get

$$k_{\min} = \frac{\pi}{a}\left(\frac{n}{N} - m\right), \quad m \in \mathbb{Z} \tag{92}$$

and if we set the square brackets equal to zero,

$$k_{\min} = \frac{1}{a}\left(\frac{\pi n}{N} \mp \arccos\left(-\frac{1}{2}\cos\left(\frac{\pi n}{N}\right)\right) - 2\pi m\right), \quad m \in \mathbb{Z}. \tag{93}$$

One of these expressions for $k_{\min}$ will give the minima and the other will give the maxima. In order to find which is which, we could differentiate $E_n^2(k_{\min})$ again. However, we can make life easier for ourselves by numerically plotting the values of $k_{\min}$ against an energy band in the dispersion, as we have done in fig. 8. From this, we can see that eq. (93) is the band minima.

7.2 Wavefunctions for the Armchair Carbon Nanotube

We are now in a position to Taylor expand about our band minima. As we want to focus on the low-energy section of the system, we can choose to work in the ground state and set $n = 0$. By substituting our armchair momentum quantisation into eq. (63), we deduce that

$$f(k) = -t\left(1 + e^{i\left(\frac{2\pi n}{Na} - k\right)a} + e^{ika}\right). \tag{94}$$

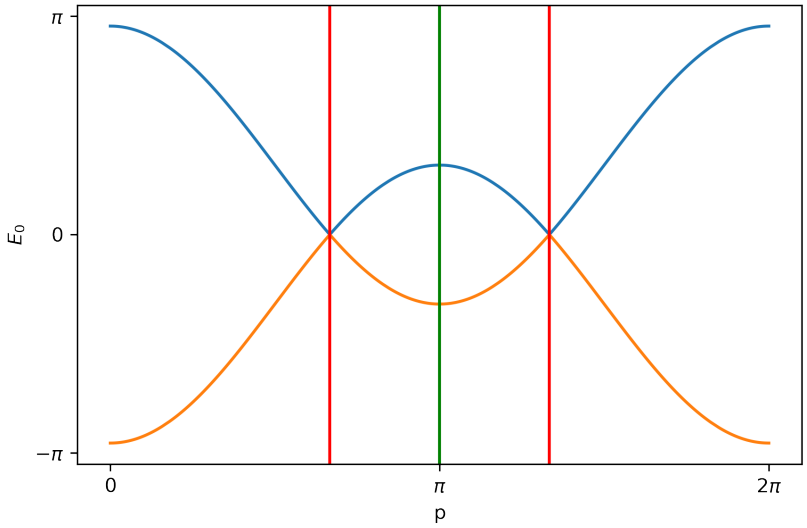

Figure 8: The energy band of the ground state $n = 0$, is shown in the blue and orange lines. The ground state turns out to be gapless for all values of N. The vertical red lines that go through the minima correspond to eq. (93) and the green line through the maxima corresponds to eq. (92).

In order to find the Taylor expansion of our Hamiltonian (eq. (75)), we need to find the terms for eq. (74) by our new expression for $f(k)$. Therefore, we differentiate $f(k)$ to get

$$f'(k) = -iat\Big(- e^{i\left(\frac{2\pi n}{Na} - k\right)a} + e^{ika}\Big) \overset{n=0}{=} -iat\Big(- e^{-ika} + e^{ika}\Big), \tag{95}$$

and then we can substitute in our minimum values of the momentum $k_{\text{min}}^{n=0}$, which gives us

$$f'(k_{\text{min}}^0) = -iat\Big(- e^{\pm i \arccos(-1/2)} + e^{\mp i \arccos(-1/2)}\Big). \tag{96}$$

From eq. (74), and using the fact that $f(k_{\text{min}}^0) = 0$, we can see that

$$\begin{aligned} f(k_{\text{min}}^0 + p) &= pf'(k_{\text{min}}^0) + \mathcal{O}(p^2) \\ &\approx -piat\Big(- e^{\pm i \arccos(-1/2)} + e^{\mp i \arccos(-1/2)}\Big) \\ &= -piat\Big(- e^{\pm i 2\pi/3} + e^{\mp i 2\pi/3}\Big) \\ &= \mp\sqrt{3}pat. \end{aligned} \tag{97}$$

Which can then be paired with eq. (75) to acquire the armchair version of the Dirac equation,

$$\begin{pmatrix} 0 & \mp\sqrt{3}pat \\ \mp\sqrt{3}pat & 0 \end{pmatrix} \begin{pmatrix} \psi_A \\ \psi_B \end{pmatrix} = E_n(p) \begin{pmatrix} \psi_A \\ \psi_B \end{pmatrix}. \tag{98}$$

We are starting to see a divergence between the zigzag and armchair cases in the non-appearance of a band gap in the Hamiltonian above. This is because the ground state of the armchair case is always gapless, regardless of the value of N. In the zigzag case, the dependence of the gap on certain values of N was directly related to the requirements for the emergence of edge states in the system.

The Hamiltonian we have found for the armchair case is given by

$$h(\boldsymbol{p}) = \mp\sqrt{3}pat \begin{pmatrix} 0 & 1 \\ 1 & 0 \end{pmatrix} = \mp\sqrt{3}pat \cdot \sigma_x, \tag{99}$$

where σ_x is the Pauli x-matrix. The eigenvalues of the Pauli x-matrix are given by ± 1, which implies that the eigenvalues of our Hamiltonian are just $\lambda_{1,2} = \pm\sqrt{3}pat$ and that the eigenvectors are the same as the ones for σ_x. This means they are given by

$$\psi_{\pm} = \frac{1}{\sqrt{2}} \begin{pmatrix} 1 \\ \pm 1 \end{pmatrix}, \tag{100}$$

with ψ_+ being the positive energy solutions. Which gives us a position space solution of the Dirac equation in the form

$$\psi(x) = \frac{1}{\sqrt{2}} \begin{pmatrix} 1 \\ 1 \end{pmatrix} e^{ipx}. \tag{101}$$

This allows us to build a forward and backward propagating wave,

$$\psi_p = \frac{1}{\sqrt{2}} \begin{pmatrix} 1 \\ 1 \end{pmatrix} e^{ipx} + \frac{R}{\sqrt{2}} \begin{pmatrix} 1 \\ 1 \end{pmatrix} e^{-ipx}. \tag{102}$$

7.3 Charge Density at the Edge

An armchair edge requires a different set of boundary conditions to the zigzag case [1]. In fact, whilst zigzag boundary conditions are generic, we find that the armchair ones are very specific and only occur for very specific edge orientations [7]. This is due to the fact that we require the normal current at the edge of the nanotube to be zero [2], but that we have a different shape for the armchair edge than we do the zigzag, and therefore we have a different set of 'missing' links. If we refer back to fig. 1 and consider rolling up our graphene into a zigzag nanotube, then we have 'missing' links at the top and the bottom where the edges are. The top and bottom edges are labelled by $x = 0$ and $x = L$. We can see in the figure that the atoms at the edge are all part of one of the A and B sub-lattices and from this, we can see where the zigzag boundary conditions (eq. (80)) come from. They do not require any equality between the different sub-lattice wavefunctions.

If we now do the same kind of thought experiment and consider rolling up the graphene in fig. 1 into an armchair nanotube. We can see that there are atoms from both sub-lattices at each

edge. This means we will require the boundary conditions to equate the wavefunctions from both sub-lattices where we didn't for the zigzag case. This leaves us with a set of boundary conditions defined by

$$\psi_A(0) = \psi_B(0) = \psi_A(L) = \psi_B(L) = 0. \tag{103}$$

We can see from these boundary conditions, that both sub-lattice wavefunctions are required to be zero at both edges of the nanotube. Given that the charge density on a nanotube is given by

$$\rho = \psi^\dagger \psi = |\psi_A|^2 + |\psi_B|^2, \tag{104}$$

We can immediately see that there can be no support for bulk states at the edge, as both ψ_A and ψ_B are required to be zero at the edge. Which can be expressed as

$$\rho(0) = \rho(L) = |\psi_A(0)|^2 + |\psi_B(0)|^2 = |\psi_A(L)|^2 + |\psi_B(L)|^2 = 0. \tag{105}$$

8 Numerical Simulation of a 1D Chain

In order to test the validity of our theoretical analysis, we will now encode our tight-binding Hamiltonian on a one-dimensional chain. A similar analysis done in [2], confirmed the support of bulk states at the edge for zigzag carbon nanotubes, the results of which are shown in fig. 6. We will use a similar numerical simulation for our armchair analysis as a way of checking the work we have already done. The benefit of simulating a one-dimensional chain compared to the full two-dimensional system, is that we can fix the momenta and focus in on of the Dirac points, as we have done in our analysis above. A two-dimensional simulation would simulate contributions from both Dirac points, which would lead to noisier wavefunctions that would be more difficult to compare to our analytical results.

In order to run such a numerical simulation, we will need to get our tight-binding Hamiltonian into a form that can be easily encoded on a computer. The first step in this will be to use a new basis. The basis we have used in our analysis helped to keep things simple, but for encoding a one-dimensional chain, we will be better off working with a Hamiltonian expressed in a Cartesian basis, $\hat{\boldsymbol{e}}_x$ and $\hat{\boldsymbol{e}}_y$. Using the same logic as we did to get eq. (56), we can use fig. 9 to derive a version of our tight-binding Hamiltonian in a Cartesian basis as

$$H = -t \sum_{\boldsymbol{r} \in A} a^\dagger_{\boldsymbol{r}} (b_{\boldsymbol{r}+\hat{\boldsymbol{e}}_{\boldsymbol{x}}-\hat{\boldsymbol{e}}_{\boldsymbol{y}}} + b_{\boldsymbol{r}-\hat{\boldsymbol{e}}_{\boldsymbol{x}}-\hat{\boldsymbol{e}}_{\boldsymbol{y}}} + b_{\boldsymbol{r}}) + \text{h.c.} \tag{106}$$

With the corresponding creation and annihilation operators expressed as

$$a^\dagger_{\boldsymbol{r}} = \frac{1}{\sqrt{N_y}} \sum_{p_y} e^{-ip_y y} a^\dagger_x(p_y), \quad b_{\boldsymbol{r}} = \frac{1}{\sqrt{N_y}} \sum_{q_y} e^{iq_y y} b_x(q_y). \tag{107}$$

As we did when we derived the dispersion relation for graphene, we can substitute the creation

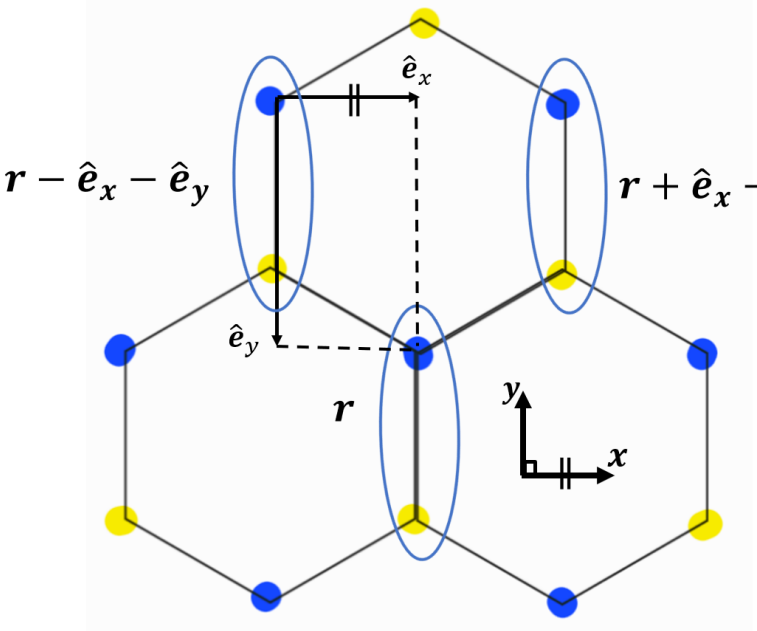

Figure 9: The graphene lattice with unit cell vectors defined in terms of a Cartesian basis. Using these vectors to define hopping between nearest neighbour sites leads to the Hamiltonian given in eq. (106).

and annihilation operators into our new Hamiltonian to get

$$\begin{aligned} H &= -\frac{t}{\sqrt{N_y}^3} \sum_{\boldsymbol{r}\in A} \sum_{p_y} \sum_{q_y} e^{-ip_y y} a_x^\dagger(p_y) \Big(e^{iq_y(y+1)} b_{x-1}(q_y) + e^{iq_y(y-1)} b_{x-1}(q_y) + e^{iq_y y} b_x(q_y) \Big) + \text{h.c.} \\ &= -\frac{t}{\sqrt{N_y}} \sum_{x} \sum_{p_y} \sum_{q_y} a_x^\dagger(p_y) \Big(e^{iq_y} b_{x-1}(q_y) + e^{-iq_y} b_{x-1}(q_y) + b_x(q_y) \Big) \Big(\frac{1}{N_y} \sum_{y} e^{i(q_y - p_y)} \Big) + \text{h.c.} \end{aligned} \tag{108}$$

where the terms in the last set of brackets equal $\delta_{p_y q_y}$. We can then use the Euler equation to simplify the exponentials in Hamiltonian, which gives us

$$\begin{aligned} H &= \sum_{p_y} \Big(-\frac{t}{\sqrt{N_y}} \sum_x a_x^\dagger \Big(2\cos(p_y) b_{x-1} + b_x \Big) + \text{h.c.} \Big) \\ &= \sum_{p_y} H(p_y). \end{aligned} \tag{109}$$

In order to encode our Hamiltonian, we want to find the single-particle Hamiltonian in terms of Dirac delta functions such that $h(\boldsymbol{p}) = h_{i,j}$. Therefore, we factor out the creation operator in $H(p_y)$ to express it in terms of delta functions,

$$H(p) = -\frac{t}{\sqrt{N}} \sum_{i,j} a_i^\dagger \Big(2\cos(p)\delta_{i-1,j} + \delta_{i,j} \Big) b_j + \text{h.c.} \tag{110}$$

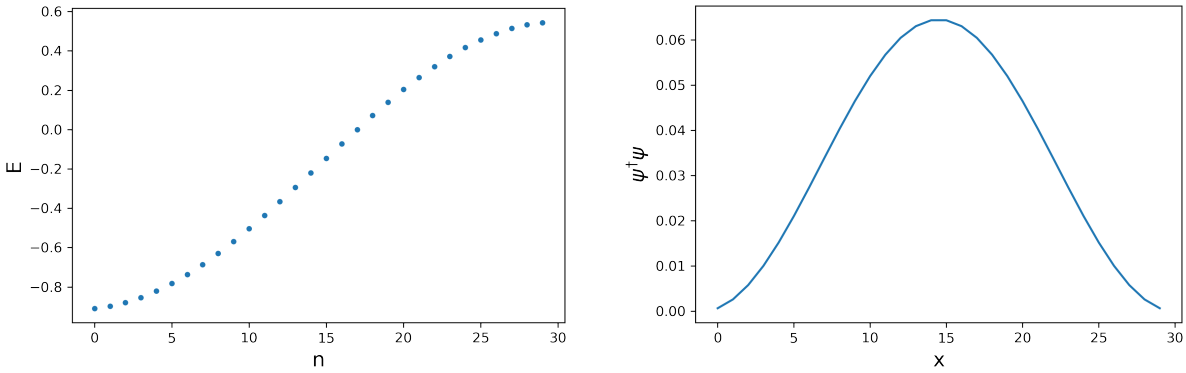

(a) Spectrum of Eigenstates

(b) Ground State Charge Density

Figure 10: Numerical simulation of a 1D chain of atoms described by our tight-binding Hamiltonian along an armchair boundary for system size $N = 30$. We find the eigenstates and eigenvalues of the single-particle Hamiltonian given in eq. (112) numerically. This allows us to plot the charge density for the ground state eigenvector. (a) shows the spectrum of possible eigenstates for our Hamiltonian and their respective eigenenergies, (b) shows the charge density for the ground state where $n = 0$.

By comparing to eq. (61), we arrive at

$$h_{i,j} = -\frac{t}{\sqrt{N}}\Big(2\cos(p)\delta_{i-1,j} + \delta_{i,j}\Big), \tag{111}$$

where we can take $p = 2\pi n/N$ as we are now quantising it in the direction of one of our basis states, as we did for the zigzag case in section 6. This gives us

$$(h_n)_{i,j} = -\frac{t}{\sqrt{N}}\left(2\cos\left(\frac{2\pi n}{N}\right)\delta_{i-1,j} + \delta_{i,j}\right) \tag{112}$$

This gives us the Hamiltonian in a form that we can encode computationally.

We have

$$H_n = \begin{pmatrix} a^\dagger & b^\dagger \end{pmatrix} \begin{pmatrix} 0 & h_n \\ h_n^\dagger & 0 \end{pmatrix} \begin{pmatrix} a \\ b \end{pmatrix} = \psi^\dagger \mathcal{H}_n \psi \tag{113}$$

as in [2]. We can now use numerical methods to diagonalise $\mathcal{H}_n$ and find its eigenvectors and eigenvalues. We can then compute the charge density from these results and plot them along the length of the chain. The results of this simulation are displayed in fig. 10. They show clear agreement with the theoretical analysis done in the previous section, as we can see the charge density has a non-relativistic profile as it goes to zero at the edges of the system.

9 Conclusion

In section 6, it was demonstrated that in zigzag carbon nanotubes we see support for the extension of bulk states to the edge. This was shown to be the result of the boundary conditions that we applied to the system. At a zigzag edge, all of the atoms belong to the same sub-lattice and the boundary conditions only require that one of the sub-lattice wavefunctions be zero at the boundary [1], leaving the other to be non-zero at the edge. The wavefunction of the entire system is a superposition of the two sub-lattice wavefunctions and therefore, we can add the charge densities of each sub-lattice together. This allows for a non-zero density of bulk states at the edge when the two sub-lattice wavefunctions have certain phases which can be controlled by the dimensions of the carbon nanotube, as shown in [2].

Contrastingly, for the armchair edge, we see that it is made up of atoms belonging to both of the triangular sub-lattices. As we design our boundary conditions in order to keep the normal current at the edge equal to zero, this means that we have to set both sub-lattice wavefunctions to be zero at the edge. By definition, the charge density is given by $\rho = \psi^\dagger \psi$ and therefore, any boundary conditions that require all of the wavefunctions to be zero at the edge, must have zero density at the edge as well.

The only true test of the validity of these results is experiment. There is currently no experimental data to support these findings, but as nanotechnology and our ability to control these systems in a laboratory setting improves, such results might be demonstrated in the future. In the meantime, the best we can say is that these results are supported by numerical simulations. The zigzag case is supported by one-dimensional chain simulations in [2] and the armchair case by the same type of simulation in section 8 of this thesis. This at least suggests that the theoretical analysis presented here has been done correctly. Furthermore, similar results for edge states existing at zigzag edges of a graphene nanoribbon have been found, along with the result that no such edge states are expected in the armchair case [16][17]. This reinforces the concept that these physical results are consequences of the edge shape, which would explain why they translate from nanotubes to ribbons and vice versa.

It will be of interest in the future to see if experiment can confirm or falsify the results of this thesis. From a theoretical point of view, it would be interesting to examine whether punctures in graphene based systems with zigzag or armchair edges offer any other counter-intuitive results. Also, to see if such research would reaffirm the results of this paper, that only the zigzag edges result in certain relativistic phenomena where the armchair ones don't. Further theoretical demonstration of this idea could reinforce the results of this thesis.

References

[1] A.H. Castro Neto, F. Guinea, N.M.R. Peres, K.S. Novoselov, A.K. Geim, *The Electronic Properties of Graphene*. Rev. Mod. Phys. 81, 109. 2009.

[2] M.D. Horner, J.K. Pachos, *Edge support of bulk states in Dirac materials due to relativity*. Phys. Rev. B 104, L081402. 2021.

[3] N. Zettili. *Quantum Mechanics: Concepts and Applications*. Second Edition. Chichester: John Wiley and Sons Ltd. 2009.

[4] M.I. Katsnelson, K.S. Novoselov, A.K. Geim, *Chiral Tunnelling and the Klein Paradox in Graphene*. Nature Phys 2, 620–625. 2006.

[5] P. Alberto, C. Fiolhais, V.M.S. Gil, *Relativistic Particle in a Box*. Eur. J. Phys. 17. 1996.

[6] W. Greiner, *Relativistic Quantum Mechanics, Wave Equations*. Third Edition. New York: Springer-Verlag Berlin Heidelberg. 2000.

[7] M.I. Katsnelson, *The Physics of Graphene*. Second Edition. Cambridge: Cambridge University Press. 2012.

[8] R. Purdy, *The Fundamentals of Particle Physics*. Luton: The Pantaneto Press, 2017.

[9] N. Stander, B. Huard, D. Goldhaber-Gordon, *Evidence for Klein Tunnelling in Graphene p-n Junctions*. Phys. Rev. Lett. 102, 026807. 2009.

[10] A.F. Young, P. Kim, *Quantum Interference and Klein tunnelling in graphene heterojunctions*. Nature Phys 5, 222–226. 2009.

[11] A. Atland, B.D. Simons, *Condensed Matter Field Theory*. Second Edition. Cambridge: Cambridge University Press. 2010.

[12] N.W. Ashcroft, N.D. Mermin, *Solid State Physics*. Fort Worth: Saunders College. 1976.

[13] A. Bohm, A. Mostafazadeh, H. Koizumi, Q. Niu, J.Zwanziger, *The Geometric Phase in Quantum Systems: Foundations, Mathematucal Concepts, and Applications in Molecular and Condensed Matter Physics*. New York: Springer-Verlag Berlin Heidelberg, 2003.

[14] B.A. Bernevig, T.L. Hughes, *Topological Insulators and Topological Superconductors*. Princeton: Princeton University Press. 2013.

[15] M. Margańska, M. del Valle, S.H. Jhang, C. Strunk, M. Grifoni, *Localization induced by magnetic fields in carbon nanotubes*. Phys. Rev. B 83, 193407. 2011.

[16] A.R. Akhmerov, C.W.J. Beenakker, *Boundary Conditions for Dirac fermions on a terminated honeycomb lattice*. Phys. Rev. B 77, 085423. 2008.

[17] K. Nakada, M. Fujita, G. Dresselhaus, M.S. Dresselhaus, *Edge states in graphene ribbons: Nanometer size effect and edge shape dependence*. Phys. Rev. B 54, 17954. 1996.

A Source Code for Plots and Numerics

Below is the code used to produce the plots and numerical simulations contained in this thesis, all of which was done using Python 3. The functionality of the code will be briefly explained.

A.1 Graphene Dispersion Relation Plot

```
1  from mpl_toolkits import mplot3d
2  import matplotlib.pyplot as plt
3  import numpy as np
4
5  t = 1
6  a = 1
7
8
9  x = np.arange(0, 2*np.pi, 0.1)
10 y = np.arange(0, 2*np.pi, 0.1)
11
12 X, Y = np.meshgrid(x, y)
13 Z = np.round(t*np.sqrt(3 + 2*np.cos(X*a) + 2*np.cos((X-Y)*a) + 2*np.cos(Y*a)), 4)
14
15
16 fig = plt.figure()
17
18 # syntax for 3-D plotting
19 ax = plt.axes(projection ='3d')
20
21 ax.plot_surface(X, Y, Z, alpha=0.5)
22 ax.plot_surface(X, Y, -Z, alpha=0.5)
23 ax.set_xlabel('$p_{1}$')
24 ax.set_ylabel('$p_{2}$')
25 ax.set_zlabel('$E(p)$')
26 plt.xticks(np.arange(0, 2*np.pi+1, step=np.pi), ['$2\pi$','$\pi$','0'])
27 plt.yticks(np.arange(0, 2*np.pi+1, step=np.pi), ['0','$\pi$','$2\pi$'])
28 ax.set_zticks([-np.pi, 0,np.pi])
29 ax.set_zticklabels(['$-\pi$','0','$\pi$'])
30 ax.view_init(0, 60)
31 plt.savefig("3D.png",dpi=300)
32 plt.show()
```

Figure 11: The code used to produce the graphene dispersion relation fig. 5.

The first 12 lines of this code serve to set up our system and figure, by defining certain values such as N and then setting up the x and y values. We then input the expression for the graphene dispersion relation as a function $z = z(x, y)$ on line 13. The rest of the code plots the 3D surface in the figure and customises the axes. On line 30, we rotate the figure in a way that best shows the Dirac cones. The final two lines produce the figure as a .png file that is used as fig. 5.

A.2 Armchair Carbon Nanotube Dispersion Relation Plot

```
1  import matplotlib.pyplot as plt
2  import numpy as np
3
4  t = 1
5  N = 20
6  a = 1
7  n = 10
8
9  for n in range(0,N):
10     x = np.arange(0, 2*np.pi, 0.0001)
11     E1 = np.round(t*np.sqrt(3 + 2*np.cos((((2*np.pi*n)/(N*a))-x)*a) + 2*np.cos((((2*np.pi*n)/(N*a))-2*x)*a) + 2*np.cos(x*a)), 4)
12     E2 = np.round(-t*np.sqrt(3 + 2*np.cos((((2*np.pi*n)/(N*a))-x)*a) + 2*np.cos((((2*np.pi*n)/(N*a))-2*x)*a) + 2*np.cos(x*a)), 4)
13     plt.plot(x,E1)
14     plt.plot(x,E2)
15
16 plt.xticks(np.arange(0, 2*np.pi+1, step=np.pi), ['0','$\pi$','$2\pi$'])
17 plt.yticks(np.arange(-np.pi, np.pi+1, step=np.pi), ['$-\pi$','0','$\pi$'])
18 plt.xlabel('p')
19 plt.ylabel ('$E_{n}$')
20
21 plt.tight_layout()
22 plt.savefig("High resoltion.png",dpi=300)
23 plt.show()
```

Figure 12: The code used to produce the dispersion relation for an armchair carbon nanotube in fig. 7.

This code works in a very similar way to the code that produces the graphene dispersion relation. The first 7 lines set up the system. The lines from 9 to 14 plot the positive and negative energy solutions in the figure for all n in the range 0 to N. Lines 16 to 19 customise the axes labels and the last three lines produce the .png file used in this thesis.

A.3 Ground State Energy Band with Minima Plot

```
1  import matplotlib.pyplot as plt
2  import numpy as np
3
4  t = 1
5  N = 20
6  a = 1
7  n = 0
8  x = np.arange(0, 2*np.pi, 0.0001)
9  E1 = np.round(t*np.sqrt(3 + 2*np.cos((((2*np.pi*n)/(N*a))-x)*a) + 2*np.cos((((2*np.pi*n)/(N*a))-2*x)*a) + 2*np.cos(x*a)), 4)
10 E2 = np.round(-t*np.sqrt(3 + 2*np.cos((((2*np.pi*n)/(N*a))-x)*a) + 2*np.cos((((2*np.pi*n)/(N*a))-2*x)*a) + 2*np.cos(x*a)), 4)
11 plt.plot(x,E1)
12 plt.plot(x,E2)
13 plt.xticks(np.arange(0, 2*np.pi+1, step=np.pi), ['0','$\pi$','$2\pi$'])
14 plt.yticks(np.arange(-np.pi, np.pi+1, step=np.pi), ['$-\pi$','0','$\pi$'])
15 for m in range(-1,0):
16     plt.axvline(x=(np.pi/a)*((n/N)-m), color = 'g', label = 'easy')
17
18 for k in range(0,1):
19     plt.axvline(x=(1/a)*((np.pi*n/N)+np.arccos(-0.5*np.cos(np.pi*n/N))-2*np.pi*k) , color = 'r', label = 'hard')
20
21 for q in range(-1,0):
22     plt.axvline(x=(1/a)*((np.pi*n/N)-np.arccos(-0.5*np.cos(np.pi*n/N))-2*np.pi*q) , color = 'r', label = 'hard')
23
24 plt.xlabel('p')
25 plt.ylabel ('$E_{0}$')
26 plt.tight_layout()
27 plt.savefig("Minima.png",dpi=300)
28 plt.show()
```

Figure 13: The code used to produce the ground state energy band plot for an armchair carbon nanotube. The code also marks the minima and maxima of the energy band by using vertical lines. This code produces fig. 8.

The first 14 lines of this code are recreating the code from the armchair dispersion plot, but only for the ground state $n = 0$. Lines 15 to 22 plot the values of eq. (92) and eq. (93) as green and red vertical lines respectively. The last five lines label the axes and produce the .png file that appears in this thesis.

A.4 Numerical Simulation of a 1D Chain

```
1  import numpy as np
2  import matplotlib.pyplot as plt
3
4  N = 20
5  n=0
6
7
8  def delta(x,y):
9      return x==y
10
11 p = np.arange(-50, 50)
12 H = np.ones((N,N))
13
14 for i in range(0,N):
15     for j in range(0,N):
16         H[i][j] = -1*(2*np.cos(2*np.pi*n/N)*delta(i-1,j) + delta(i,j))/(np.sqrt(N))
17
18 D,U = np.linalg.eigh(H)
19
20 plt.plot(D, '.')
21 plt.xticks(np.arange(0,21,step=1))
22 plt.xlabel('n', fontsize = 15)
23 plt.ylabel('E', fontsize = 15)
24 plt.tight_layout()
25 plt.savefig("Eigenstates.png",dpi=300)
26 plt.show()
27
28 psi = np.abs(U[:,0])**2
29
30 plt.plot(psi)
31 plt.xticks(np.arange(0,21,step=1))
32 plt.xlabel('x', fontsize = 15)
33 plt.ylabel('$\psi^{\dagger}\psi$', fontsize = 15)
34 plt.tight_layout()
35 plt.savefig("Density.png",dpi=300)
36 plt.show()
```

Figure 14: The code used to numerically simulate an armchair system on a 1D chain in fig. 10.

The first 5 lines of this code set up the system. Lines 8 and 9 define a function that we can use as a Dirac delta function. From line 11 to 16, we create a the matrix version of our Hamiltonian out of eq. (112). Line 18 then calculates the eigenstates and eigenvalues. The following lines up to line 26 then plots the eigenstates against the eigenvalues. Line 28 calculates the density before the rest of the code plots it against the system size.